Surface Rupture of Multiple Crustal Faults in the M_w 7.8 2016 Kaikōura Earthquake, New Zealand

by Nicola J. Litchfield*, Pilar Villamor, Russ J. Van Dissen, Andrew Nicol, Philip M. Barnes, David J. A. Barrell, Jarg R. Pettinga, Robert M. Langridge, Timothy A. Little, Joshu J. Mountjoy, William F. Ries, Julie Rowland, Clark Fenton, Mark W. Stirling, Jesse Kearse, Kelvin R. Berryman, Ursula A. Cochran, Kate J. Clark, Mark Hemphill-Haley, Narges Khajavi, Katie E. Jones, Garth Archibald, Phaedra Upton, Cameron Asher, Adrian Benson, Simon C. Cox, Caleb Gasston, Dan Hale, Brendan Hall, Alexandra E. Hatem, David W. Heron, Jamie Howarth, Tim J. Kane, Geoffroy Lamarche, Steve Lawson, Biljana Lukovic, Samuel T. McColl, Christopher Madugo, John Manousakis, Duncan Noble, Kate Pedley, Katrina Sauer, Timothy Stahl, Delia T. Strong, Dougal B. Townsend, Virginia Toy, Jack Williams, Suzanne Woelz, Robert Zinke

* GNS Science, PO Box 30-368, Lower Hutt 5040, New Zealand, n.litchfield@gns.cri.nz

Electronic supplement: Table S1 – additional data on the Kaikōura earthquake surface-rupturing faults, Fig. S1 – 3D pdfs of the 3D geological fault model.

Abstract Multiple (>20) crustal faults ruptured to the ground surface and seafloor in the 14 November 2016 M_w 7.8 Kaikōura earthquake, and many have been documented in detail, providing an opportunity to understand the factors controlling multi-fault ruptures, including the role of the subduction interface. We present a summary of the surface ruptures, as well as previous knowledge including paleoseismic data, and use these data and a 3D geological model to calculate cumulative 'geological' moment magnitudes (M_w^G) and seismic moments for comparison with

those from geophysical datasets. The earthquake ruptured faults with a wide range of orientations, sense of movement, slip rates and recurrence intervals, and crossed a tectonic domain boundary, the Hope fault. The maximum net surface displacement was ~12 m on the Kekerengu and the Papatea faults, and average displacements for the major faults were 0.7–1.5 m south of the Hope fault, and 5.5–6.4 m to the north. $M_w{}^G$ using two different methods are $M_w{}^G$ 7.7 $^{+0.3}_{-0.2}$ and the seismic moment is 33–67% of geophysical datasets. However, these are minimum values and a best estimate $M_w{}^G$ incorporating probable larger slip at depth, a 20 km seismogenic depth, and likely listric geometry is $M_w{}^G$ 7.8 ± 0.2, suggests ≤32% of the moment may be attributed the slip on the subduction interface and/or a mid crustal detachment. Likely factors contributing to multi-fault rupture in the Kaikōura earthquake include: (1) the presence of the subduction interface; (2) physical linkages between faults; (3) rupture of geologically immature faults in the south; and (4) inherited geological structure. The estimated recurrence interval for the Kaikōura earthquake is ≥5000-10,000 years, and so it is a relatively rare event. Nevertheless, these findings support the need for continued advances in seismic hazard modelling to ensure that they incorporate multi-fault ruptures that cross tectonic domain boundaries.

Introduction

Coseismic rupture of multiple crustal faults has been recorded for several historical earthquakes worldwide (Matsuda, 1974; Wallace, 1984; Beanland et al., 1989; Sieh et al., 1993; Kurushin et al., 1997; Meng et al., 2012; Beavan et al., 2012; Schwartz et al., 2012; Fletcher et al., 2014). The complexity of such multi-fault ruptures is now being documented in unprecedented detail, using techniques such as lidar differencing (e.g., Oskin et al., 2012) and subpixel optical image correlation (e.g., Zinke et al., 2014), as well as the integration of multiple geological (e.g.,

field mapping) and geophysical (e.g., seismology, InSAR) techniques (e.g., Goto et al., 2017; Hamling et al., 2017). The use of new and multiple techniques contributes to better understanding of the factors controlling multi-fault ruptures, which in turn contribute to understanding fault interactions, earthquake processes, and refining seismic hazard assessment.

Multiple (>20) crustal faults ruptured to the ground surface and seafloor in the 14 November 2016 M_w 7.8 Kaikōura earthquake (Litchfield et al., 2016; Hamling et al., 2017; Kaiser et al., 2017; Stirling et al., 2017; Kearse et al., 2018; Langridge et al., 2018; Nicol et al., 2018; Williams et al., 2018; this study) (Fig. 1b). Some of these faults had very large (≤12 m) net surface displacements (Kearse et al., 2018; Langridge et al., 2018; this study). Large surface displacements on faults such as the Kekerengu fault are consistent with interpretations from some geophysical studies that it was rupture of this fault that released much of the Kaikōura earthquake seismic moment (e.g., Hamling et al., 2017; Holden et al., 2017; Hollingsworth et al., 2017). There is also evidence that the Hikurangi subduction interface and/or a mid crustal detachment ruptured in the Kaikōura earthquake. The subduction interface had been interpreted to be permanently locked (i.e., not able to slip) beneath the northeastern South Island (e.g., Reyners, 1998). Datasets used to interpret a shallow-dipping deep rupture include initial global moment tensors, teleseismic, geodetic, InSAR, local strong ground motion, coastal uplift, and tsunami datasets (e.g., Duputel and Rivera, 2017; Bai et al., 2017; Cesca et al., 2017; Clark et al., 2017; Wallace et al., 2017a; Wang et al., 2018; Wen et al., 2018; Zheng et al., 2018). Assessing the role of the Hikurangi subduction interface rupture in the Kaikōura earthquake has relevance to the potential of multi-fault ruptures in subduction settings worldwide.

In this paper we present a synthesis of the surface (crustal) fault ruptures in the Kaikōura earthquake, summarizing the details from papers in this volume on the major faults (Kearse et al.,

2018; Langridge et al., 2018; Nicol et al., 2018; Williams et al., 2018), along with the minor ruptures, previous knowledge and paleoseismic history. We combine the surface rupture data with geological and some geophysical data to develop a 3D geological fault model to examine possible linkages between the crustal faults and the Hikurangi subduction interface. We use this information to calculate range of 'geological' seismic moments (M_o^G) and moment magnitudes (M_w^G), which are compared with published estimates mainly based on geophysical data. These analyses provide a useful basis to consider factors contributing to multi-fault rupture, insights into the relative role of rupture of crustal faults versus the subduction interface or a mid crustal detachment, and implications for seismic hazard modelling for one of the most complex historical large earthquakes.

Tectonic and Geologic Setting

The Kaikōura earthquake occurred in the transition zone between westward-subduction of the Pacific plate at the Hikurangi subduction margin in the northeast and the continental collision along the transpressional Alpine fault in the southwest (Fig. 1a). The transition zone has been divided into several crustal tectonic domains, based on their differing fault kinematics and slip rates (Pettinga et al., 2001; Stirling et al., 2012; Litchfield et al., 2014). The domains arise largely because of the late Neogene overprint of the largely strike-slip Marlborough fault belt on a region with structure related to extensional tectonics in the late Cretaceous and contractional tectonics in the Neogene (Little and Jones, 1998, Rattenbury et al., 2006).

The earthquake initiated in the predominantly contractional North Canterbury Domain (NCD), and extended northeastward into the dextral strike-slip Marlborough Fault System (MFS) domain (Fig. 1a). Faults in the NCD are predominantly northeast-striking, range-bounding,

oblique-reverse and thrust faults with relatively low slip rates (≤2 mm/yr) (e.g., Nicol et al., 1995; Barnes, 1996; Pettinga et al., 2001; Nicol et al., 2018). Surface fault dips in the range of 15 to 70° have been observed, with numerous antithetic faults, thrust wedges and asymmetric anticlines (Cowan et al., 1996; Pettinga et al., 2001; Litchfield et al., 2003) and structural interpretations often infer a listric geometry (Rattenbury et al., 2006; Vanderleest et al., 2017). Across the NCD a cumulative net slip rate of 2.3 ± 0.7 mm/yr has been calculated along the transect shown in Fig. 1a (Litchfield et al., 2014). The relatively youthful faults in the NCD (e.g., Nicol et al. 1994; Barnes 1996; Cowan et al. 1996; Pettinga et al. 2001; Litchfield et al. 2003, 2014; Vanderleest et al., 2017) are considered to reflect the ongoing southward encroachment of the plate boundary deformation.

The MFS faults are more continuous, variably cutting through and uplifting, the Kaikoura ranges (e.g., Van Dissen and Yeats, 1991; Nicol and Van Dissen, 2002) (Fig. 2). The total strike-slip motion on each of the faults of the MFS is, with the exception of the Wairau fault, less than several tens of kilometers. Thus, the surface traces, despite now having overall high slip rates (individual faults have slip rates ≤25 mm/yr) are complex with immature principal displacement zones. The cumulative net slip rate across the MFS is 37.8 ± 3.4 mm/yr (Fig. 1a) (Litchfield et al., 2014). The age of the MFS has been interpreted to decrease southward, possibly reflecting southward migration of the Hikurangi subduction margin and progressive development of the MFS (e.g., Yeats and Berryman, 1987; Little et al., 1998; Wallace et al., 2007).

Prior to the Kaikōura earthquake, there was debate as to the ongoing activity of the Hikurangi subduction interface beneath the northeastern South Island region. Some workers considered this southern end of the subduction zone to be permanently locked, with plate motion entirely accommodated by the crustal faults (e.g., Reyners, 1998; Reyners et al., 2017). Others have argued that long-term average rates of slip on the subduction zone could be on the order of a

few mm/yr (Wallace et al., 2012). Pre-Kaikōura earthquake seismological data suggested that the base of the seismogenic crust is at a relatively uniform depth of about 15 ± 5 km, particularly west of the Kaikōura ruptures, where there were more data (Eberhart-Phillips and Bannister, 2010). That depth range was used in the 2010 version of the New Zealand National Seismic Hazard Model (hereafter referred to as the 2010 NSHM) for the base of the seismic fault sources in this region (Stirling et al., 2012). However, a 3D velocity model of the northern South Island shows that properties such as *Vp* are highly variable at depth in the vicinity of Kaikōura, with abrupt changes across some faults that likely reflect large finite translations of crustal blocks through geological time (Eberhart-Phillips and Bannister, 2010; Ellis et al, 2017). Relocations of Kaikōura earthquake aftershocks are still ongoing, but initial locations show aftershocks from the Kaikōura earthquake down to 25 km (Kaiser et al. 2017; Cesca et al. 2017; Nicol et al., 2018).

The main geological units of the area can be divided into Mesozoic basement rocks beneath most of the high ranges, overlain by a Late Cretaceous – Quaternary cover sequence preserved on the lower slopes and in the valleys (Fig. 2) (Rattenbury et al., 2006; Edbrook et al., 2015). The basement is dominated by quartzofeldspathic marine sandstone (greywacke) and mudstone deposited in an earlier subduction zone, and deformed in an accretionary wedge and during convergent tectonism in the middle Jurassic to late Early Cretaceous (Rattenbury et al., 2006). The Mesozoic deformation resulted in a pervasive structural grain that is overall north to northeast-striking in the area of the Kaikōura earthquake. The cover sequence consists of mainly marine sandstones, mudstones and limestones deposited during a transgression and regression sequence during an era of relative tectonic quiescence, followed by further regression and ultimately deposition of fluvial deposits following uplift and erosion associated with development of the modern plate boundary in the Neogene.

Overview of the 2016 M_w 7.8 Kaikōura Earthquake and Fault Source Models

The Kaikōura earthquake initiated near the township of Waiau (Fig. 1b), on a previously unmapped part of The Humps fault (Cesca et al., 2017; Nicol et al., 2018). The rupture propagated generally unilaterally north-eastward (Cesca et al., 2017; Duputel and Rivera, 2017; Kaiser et al., 2017; Zhang et al., 2017) and produced surface displacements on a complex network of crustal faults that crossed the coast in several places (Figs. 1b, 3b-d) (Litchfield et al., 2016; Hamling et al., 2017; Clark et al., 2017; Stirling et al., 2017; Kearse et al., 2018; Langridge et al., 2018; Nicol et al., 2018; Williams et al., 2018; this study). The rupture terminated northeastwards in an area of heightened seismicity following two M_w 6.6 earthquakes in 2013 (Fig. 1b) (The Cook Strait earthquakes; Holden et al., 2013). This area may also coincide with the approximate location of the southern termination of the great (~M_w 8.1) 1855 Wairarapa earthquake (Little et al., 2018), although it has also been suggested that the 1855 rupture also involved the Needles fault (Grapes and Holdgate, 2014). The Kaikōura earthquake lasted for ≥90 s, and consisted of several sub-events (e.g., Duputel and Rivera, 2017; Kaiser et al., 2017; Hollingsworth et al., 2017; Holden et al., 2017), and the overall rupture speed was slower than most crustal earthquakes (≤2.0 km/s; Cesca et al., 2017; Holden et al., 2017; Hollingsworth et al., 2017 Kaiser et al., 2017; Kaneko et al., 2017; Wen et al., 2018), which may be a consequence of the multi-fault rupture. Horizontal and vertical peak ground accelerations (PGAs) exceeded 1 g at both ends of the rupture (Bradley et al., 2017; Kaiser et al., 2017).

In addition to ground surface rupture, the Kaikōura earthquake was associated with: (1) vertical ground deformation manifested along ~110 km of coastline (Figs. 1b, 2c and d), mainly as uplift of ≤6.5 m with some local subsidence of ≤2.5 m (Clark et al., 2017); (2) a tsunami with a

local run-up of ≤6.9 m (Power et al., 2017); (3) an anomalously large slow slip event along much of the Hikurangi subduction margin and possible afterslip in the Kaikōura earthquake region (Wallace et al., 2017a,b); (4) localized areas of liquefaction (Stringer et al., 2017; Bastin et al., 2018); and (5) >10,000 landslides (Dellow et al., 2017; Massey et al., 2018). The coastal deformation is mostly attributed to displacement on ground surface-rupturing faults. However, broad, low amplitude (<1 m) coastal uplift seen along the ~25 km length of coastline surrounding Kaikōura Peninsula is inferred to be the result of displacement on the shallow northwest-dipping reverse Kaikōura Peninsula fault lying offshore southeast of the Peninsula (Clark et al., 2017) (Fig. 2).

A series of fault rupture models have been developed for the Kaikōura earthquake and are summarized in Table 1. The number of fault sources in each model varies from 2 to 21, representing up to 12 of the crustal faults defined in this study. All models include the Kekerengu fault (generally with the Needles fault and Jordan thrust) and most include The Humps and Hundalee faults (generally with the southern section of the Leader fault). Half of the models explicitly include a Hikurangi subduction interface source (Bai et al., 2017; Duputel and Rivera, 2017; Hamling et al., 2017; Wang et al., 2018; Wen et al., 2018), and one (Hollingsworth et al., 2017) includes a thrust fault that they note could be the interface, or a shallow-dipping crustal fault such as the Kekerengu Bank Thrust fault. Cesca et al. (2017) model a mid crustal shallow dipping fault, but note they cannot discriminate whether this thrust is linked to the interface or not. The contribution of rupture of the subduction interface source ranges from 9% by Hamling et al. (2017) to 60% by Bai et al. (2017) (Table 1).

Methods and Data

Surface Rupture Mapping

Onshore surface ruptures were initially identified from helicopter surveys (Fig. 3c, e) starting within hours of the earthquake. Field surveying of the surface rupture traces was undertaken using hand-held Global Positioning System (GPS) and Real Time Kinematic (RTK) GPS equipment. Horizontal and vertical displacements of natural and anthropogenic features were measured in the field using tape measure, RTK GPS (horizontal accuracy of 1–2 cm, vertical 2–3 cm) and, at selected sites, Unmanned Aerial Vehicles (UAV) with ground control points obtained using RTK GPS. Three-dimensional structure-from-motion (SfM) Digital Surface Models (DSMs) of about 5 cm resolution were constructed for the UAV data using Agisoft Photoscan.

Aerial photograph and Light Detection and Ranging (lidar) surveys with sub-meter resolution were collected starting 19 November 2016 and cover almost the entire region of surface rupture shown in Fig. 1b (the exception is part of the Manakau fault). One meter and 20 cm pixel Digital Elevation Models (DEMs) and Digital Terrain Models (hill-shaded) were developed from the processed lidar data. In selected areas (particularly along the coastline and a portion of the Papatea fault) a topographic difference model was developed by subtracting the post-earthquake and pre-existing lidar data (acquired in 2012) (for further details see Clark et al., 2017, and Langridge et al., 2018).

The first seafloor surface rupture survey was undertaken 19–21 November 2016 on the RV Tangaroa and focused on the northern section of the Needles fault. Multibeam bathymetry surveying was undertaken with a hull-mounted Kongsberg EM302 and POSMV navigation and motion compensation system. The bathymetry survey was supported by acoustic profiling using a hull-mounted PS18 TOPAS parametric sub-bottom profiler. Data were processed using CARIS

HIPS and gridded at 2 m resolution. A second survey to obtain further information on submarine fault ruptures was undertaken during 6–13 January 2017 on the RV Ikatere. The surveying was undertaken using a Kongsberg EM2040 multibeam echosounder system and an Applanix POS/MV 320 motion sensor (>20 m water depth), and a PS120 TOPAS parametric sub-bottom profiler (10–20 m water depth). The multibeam data were also processed in CARIS HIPS, with grids of the processed data prepared at 0.5 and 2 m DEM scales, depending on water depth and acoustic system. Examples of the multibeam bathymetry and sub-bottom profile data are presented in Kearse et al. (2018).

A combined onshore-offshore 1:250,000 scale map was developed summarizing the entire surface rupture dataset (Fig. 1b) and is available for download from the New Zealand active faults database (see Data and Resources section; Langridge et al. 2016).

Maximum and Average Displacement Calculations

Field measurements of vertical and horizontal surface rupture displacements were supplemented by measurements from lidar DTMs and DEMs; details of the measurement methods are described by Kearse et al. (2018), Langridge et al. (2018), Nicol et al. (2018) and Williams et al. (2018). The number of measurements for each fault varies significantly depending on accessibility and availability of markers. In this summary, we present a maximum net displacement for each fault, which was calculated from the horizontal and vertical displacements and an adopted representative fault dip value (Table 2; grid references of the maximum net displacement locations are given in Table S1 in the electronic supplement to this article). Fault dip data was sourced from: field measurements; Kaikōura earthquake source models (e.g., Hamling et al., 2017; Clark et al., 2017); bedrock fault measurements (Rattenbury et al., 2006); and/or relationships of fault traces

to topography. A single dip value for each of the faults is a simplification, and it is likely that the dip of at least some of the reverse faults decreases with depth, particularly where they approach the subduction interface (e.g., Barnes and Audru, 1999). The adopted dip values are considered to be the best overall representation for each fault and uncertainty estimates are also provided (Table 2). We use this maximum net displacement to separate faults into those with major (>1.5 m) and minor (≤1.5) surface rupture displacement (Table 2). The use of 1.5 m is purely arbitrary and the division is predominantly for descriptive purposes, although it likely broadly reflects earthquake processes as briefly discussed. For faults with slip distributions (described next), we also calculate the percentage of the length of the fault that the displacement is greater than half the maximum displacement (%L½D_{max}), as an indication of the relationship between the maximum displacement and displacement along the remainder of the fault (i.e., whether it's a localized, anomalously high value, or not).

Slip distributions have been developed for 10 of the major faults (The Humps, Leader, Conway-Charwell, Stone Jug, Hundalee, Papatea, Upper Kowhai, Manakau, Kekerengu, Needles – vertical only) and the details are presented in Kearse et al. (2018), Langridge et al. (2018), Nicol et al. (2018) and Williams et al. (2018). In this summary, we present net slip distributions for these faults (Fig. 4). For the Papatea and Hundalee faults, for which net slip distribution curves are not presented in the detailed papers, the curves were derived from the vertical and horizontal slip distributions using a single dip value with uncertainties (Table 2; the same as used for the maximum dip calculations). The net slip distributions are used to calculate an average surface rupture displacement (D_{ave}), which for those not presented in the detailed papers (Hundalee) or presented using a different method (Papatea), are calculated by dividing the area beneath the

distribution by fault length (Tables 2 and 3). The average (net) surface rupture displacements are listed in Tables 2 and 3.

3D Geological Fault Model Development

An improved understanding of the complexity of the Kaikōura earthquake requires not only the surface rupture pattern but also the fault pattern at seismogenic depth. Although still overly simplistic we have constructed a 3D model for the major faults using Leapfrog Geo® software (Figs. 5 and S1 in the electronic supplement to this article) to examine possible linkages between the crustal faults and the Hikurangi subduction interface. It includes some major faults that didn't rupture in the Kaikōura earthquake (e.g., the Clarence fault) to provide a picture of the broader kinematic setting.

The surface geometry of each major crustal fault was generalized and straightened from the mapped surface rupture traces and modeled into a simplified plane fitted to the inferred dip and dip direction used for the maximum net displacement calculations (Table 2). Each is modelled as a planar fault plane, whereas, as noted above, many could be listric at depth, but there is currently no data to constrain such a geometry. In support of this possibility we note that the deep structure of the Wairarapa fault in the southern North Island that ruptured with a M8.2 earthquake in 1855 and had a maximum of 18 m of dextral displacement (Rodgers and Little, 2006) has a listric geometry (Henrys et al., 2013). Laterally, each fault plane is taken either to terminate directly against another fault plane, or to end arbitrarily against an imaginary vertical plane (e.g., at the end of the fault). The base of each crustal fault plane is set at either 20 km depth or at the subduction interface (whichever is shallower). The 20 km depth is considered to represent the maximum depth of the base of the seismogenic zone (Eberhart-Phillips and Bannister, 2010;

Stirling et al., 2012) in this region, based on background seismicity, but this may be an underestimate of how deep ruptures may extend during large earthquakes (e.g., Wesnousky, 2008; Beeler et al., 2018).

The subduction interface geometry is from Williams et al. (2013) and is considered to have a depth uncertainty of ±5 km (S. Bannister personal communication, 2017). The slip patch on the subduction interface is from Clark et al. (2017). Figure S1a in the electronic supplement to this article contains a 3D pdf of the model, and Figure S1b shows the same model with the addition of the Vp = 6 km/s isosurface (Ellis et al., 2017) to examine whether variations in crustal properties at seismic depths may have influenced the complexity of the rupture.

Geological Seismic Moment and Moment Magnitude Calculations

Estimates of geological moment magnitude (M_w^G) for the Kaikōura earthquake are calculated using two methods. The first starts with calculating a geological seismic moment (M_o^G) from average displacement (D_{ave}) using the equation by Aki and Richards (1980):

$$M_o = \mu LWD \quad (1)$$

where μ is rigidity modulus (assumed to be 3×10^{10} N/m^2), L is fault length in meters, W is fault width in meters, and D is displacement in meters. L is from the field mapping (Table 2), and the minimum and maximum values (Table 3) are inferred from the shortest and longest possible ruptures (e.g., taking into account junctions with other faults) where possible. Where not possible, a default uncertainty of ±10% is applied as used in the 2010 NSHM (Stirling et al., 2012). W is the depth to the base of the seismogenic zone in this region from pre-Kaikōura earthquake data (Eberhart-Phillips and Bannister, 2010; Stirling et al., 2012), and is fixed at 15 ± 5 km for all faults. D is the average surface rupture displacement (D_{ave}) calculated for 10 of the major faults using the

net slip distributions as described above. The seismic moment (M_o) for each fault is then summed and the overall geological moment magnitude, M_w^G, is calculated using the equation of Hanks and Kanamori (1979):

$$\log M_o = 16.05 + 1.5M_w \quad (2)$$

A moment magnitude (M_w) is also calculated for each fault by again using equation 2.

The second method starts with calculating moment magnitude (M_w) for each fault using the New Zealand scaling relationship for faults in this area in the National Seismic Hazard Model (Stirling et al., 2008, 2012):

$$M_w = 4.18 + 2/3\log W + 4/3\log L \quad (3)$$

whereby L is fault length in kilometers and W is fault width in kilometers (note the different units to equation 1). These are calculated as described for equation 1 above. The M_w for each fault are then converted to geological seismic moment (M_o^G) using equation 2, which are summed, and the cumulative moment magnitude (M_w^G) is calculated again using equation 2.

The M_o^G and M_w^G estimates calculated from both methods are summarized in (Table 3), but are minimum values. There are several reasons for this: (1) average displacement (D_{ave}) is not available for all of the surface-rupturing faults (method 1), (2) D_{ave} is the average displacement at the ground surface and the displacement at depth could be larger (we note that some Kaikōura earthquake fault source models require very large slip at depth – double that of maximum surface slip), (3) the fault planes are treated as planar, whereas they could in reality have a curved (listric) geometry, and therefore have a larger W, and (4) the seismogenic rupture depths may have been deeper during the earthquake (e.g., Nicol et al., 2018), which would also result in a larger W. In order to provide what we consider to be best estimates of M_o^G and M_w^G taking into account for the factors detailed above, we also calculate M_o^G and M_w^G using some geologically reasonable values

in Table 4. These values are: (1) a subsurface displacement 1.4× the surface displacement (i.e., a surface to sub-surface slip ratio of 0.7; a median value of the range documented for both immature and mature faults by Dolan and Haravitch (2014)), (2) a 20 ± 5 km seismogenic depth (as used in the 3D model and from The Humps Fault aftershock modelling, Nicol et al. (2018)), and (3) a 45° ± 10° dip to approximate a listric fault.

Kaikōura Earthquake Surface Ruptures and Paleoseismic History

Our detailed mapping has revealed that over 20 faults with surface displacements of >0.5 m ruptured the ground surface or seafloor (Fig. 1b; Table 2); the exact number of surface ruptures remains uncertain because of the inherent challenges, and at times controversy, of defining individual discrete faults (see the discussion in the Appendix). The total crustal fault surface rupture length, approximated by two simplified, *en echelon* straight-line segments, the southern one striking east-northeast and the northern one striking northeast, is ~165 km. Below we describe the surface ruptures from southwest to northeast, in approximately the order in which they ruptured, as well as previous information for each fault. Paleoseismic data is summarized in Tables 4 and 5, and the faults included in the 2010 NSHM are summarized in Table S1 in the electronic supplement to this article.

North Canterbury Domain Surface Ruptures

The Humps fault

Approximately 36 km of rupture occurred on The Humps fault (Fig. 1b; Nicol et al., 2018). The rupture can be divided into two sections – a 20-km-long, west-striking, steeply south-dipping, section (The Humps West) cutting through Quaternary gravels of the Emu Plains, and a 16-km-

long more northeast-striking, moderately northwest-dipping section (The Humps East) on the south side of the basement-cored Mt Stewart Range (Figs. 1b, 2, Table 2; Nicol et al., 2018). At its eastern end, the fault intersects the Leader fault at a high angle (Figs. 1b, 2, 5). Displacement was primarily reverse-dextral on The Humps West fault and dextral-reverse on The Humps East. The displacement also varies along its length (Fig. 4; Nicol et al., 2018) – the maximums are 3.9 (3.5–4.4) m and 4.1 (3.2–5.3) m on The Humps West and East, respectively (Fig. 1b; Table 2), and the average displacement (both segments) is 1.5 (1.2–1.7) m (Fig. 4; Table 3). The maximum displacements are relatively localized, as shown by the $\%L_{½D_{max}}$ of 21% (both strands) (Table 2).

The Humps fault east of Waiau (Fig. 1b) had been mapped prior to the Kaikōura earthquake (Rattenbury et al., 2006; Barrell and Townsend, 2012) and an extension to the west was considered possible. It had not been included in the 2010 NSHM (Stirling et al., 2012, 2017). A slip rate of 0.2 ± 0.1 mm/yr has been estimated from scarp heights on terraces of inferred age (Barrell and Townsend, 2012; Table 5). Observations made during the surface rupture mapping fieldwork suggests that there has been at least one event during the Holocene, and the recurrence interval is inferred to be 5000–10,000 years (Table 5). Paleoseismic studies of The Humps fault are currently underway.

Leader fault

Rupture on the 28-km-long Leader fault comprises a complex, broadly NNE-striking network of ruptures that extends north and south of the eastern end of The Humps Fault and at its northern extent links to the Conway-Charwell fault (Figs. 1b, 2, 3a, 5). The 18-km-long southern section strikes northeast and has a shallow dip to the northwest, in places following the basement–Tertiary contact (Fig. 2), and so may accommodate some bedding-parallel slip (Nicol et al., 2018). In contrast, the 10-km-long northern section is overall more northerly, and in the north is entirely

within basement and follows basement bedding. Displacements were highly variable (Fig. 4), but are overall sinistral-reverse, and the average displacement is 1.2 (1.0–1.5) m (Table 3; Nicol et al., 2018). The maximum net displacement of 4.0 (3.5–4.4) m (Fig. 1b; Table 2) was recorded at a site locally referred to as the Waiau or Woodchester Wall, but is a localized feature (%L½D_{max} = 6%) and may be enhanced by gravitational effects (landsliding; Nicol et al., 2018).

The Leader fault was not recognized prior to the Kaikōura earthquake and so was not included in the 2010 NSHM (Stirling et al., 2012). There are no paleoseismologic data for this fault, but work is currently underway.

Conway-Charwell fault

A ~5 km long, northeast-striking, rupture occurred on the Conway-Charwell fault, which is subparallel to, ~1–2 km south of, and dips steeply towards, the Hope fault (Figs. 1b, 5). The western and eastern ends terminate against the Leader and Stone Jug faults, respectively (Figs. 1b, 2). The center of the fault displaces basement rocks and the ends displace Quaternary deposits (Nicol et al., 2018) (Fig. 2). Displacement was oblique-reverse, with a maximum net displacement of 1.6 (1.3–1.9) m (Fig. 1b; Table 2). Only a few displacement measurements have been obtained (Fig. 4; Nicol et al., 2018), but from these an average displacement of 0.7 (0.5–0.9) m has been calculated (Table 3). The %L½D_{max} is 32%.

The Conway-Charwell fault had been mapped prior to the Kaikōura earthquake (Rattenbury et al., 2006; Barrell and Townsend, 2012), but was not explicitly included in the 2010 NSHM because of its short length and close proximity to the Hope fault (Stirling et al., 2017). A slip rate of 0.05–2 mm/yr has been estimated from scarp heights on terraces of inferred age (Barrell and Townsend, 2012; Table 5). A recurrence interval of ≥6000 years and a previous surface rupture event within the Holocene is inferred from field observations of where it crosses fluvial terraces

(Barrell and Townsend, 2012). Paleoseismic studies of the Conway-Charwell fault are currently underway.

Stone Jug fault

Approximately 18 km of north-northwest-striking rupture occurred on the Stone Jug fault between the Conway-Charwell fault in the north to the Hundalee fault in the south (Figs. 1b, 2, 5). In the north it cuts through Quaternary gravels, but in the center and south it is in basement rocks (Fig. 2), where, like the Leader fault, it follows basement bedding (Nicol et al., 2018). Due to the inaccessibility and lack of markers only a few displacement measurements are available (Nicol et al., 2018), but it is overall sinistral with a variable component and sense of vertical movement, and the maximum net displacement is 0.8 (0.7–0.9) m (Fig. 1b; Table 2).

The northern end of the Stone Jug fault had been mapped prior to the Kaikōura earthquake but was included as part of the Conway-Charwell fault (Rattenbury et al., 2006; Barrell and Townsend, 2012). Observations made during the surface rupture mapping suggest that the last event prior to the Kaikōura earthquake was almost certainly within the Holocene, and the recurrence interval could be on the order of 6000 years (Table 5).

Hundalee fault

Surface rupture occurred on ~14 km of the northeastern part of the northeast-striking, steeply northwest-dipping, Hundalee fault; ~12 km along the southeast side of a basement-cored range, and ~2 km of submarine rupture to Kaikōura canyon (Figs. 1b, 2, 3b, 5; Williams et al., 2018). The Hundalee fault forms the southern boundary of significant coastal uplift (Figs. 1b, 3b) (Clark et al., 2017). Displacement was predominantly dextral at the coast but displayed dip-slip and dominantly sinistral movement at other sites along the onland portion (Williams et al., 2018).

The maximum net displacement of 4.0 (3.4–4.7) m is a relatively localized feature where it crossed the coast (%L½D$_{max}$ = 17%) and the average displacement is 1.2 (0.9–2.7) m (Figs. 1b, 4, Table 2).

The Hundalee fault was well known prior to the earthquake (e.g., Warren, 1995; Pettinga et al., 2001; Rattenbury et al., 2006; Barrell and Townsend 2012), but the Kaikōura earthquake rupture was confined to the northeastern part of the ~30-km-long-fault (Williams et al., 2018). A ~50-km-long Hundalee fault source, extending offshore to Kaikōura Peninsula, had been included in the 2010 NSHM (Stirling et al., 2012). A slip rate of 1.2 $^{+1.2}_{-0.8}$ mm/yr has been calculated from displacement of fluvial terraces of inferred age (Ota et al., 1996; Pettinga et al., 2001; Litchfield et al., 2013, 2104), and a recurrence interval of 3080 $^{+7075}_{-1630}$ years calculated for the fault source in the 2010 NSHM (Stirling et al., 2012; Table 5). The most recent event prior to the Kaikōura earthquake is inferred to have been during the Holocene. Paleoseismic studies of the northeastern onshore Hundalee fault are currently underway.

Whites fault

A series of discontinuous north-striking ruptures extend from a point ~5 km north of the coast and the eastern end of the Hundalee fault to near the Hope fault (Fig. 1b), and have been tentatively called the Whites fault. They are in a mountainous area covered by thick forest cover and so have been mapped using lidar data and viewed from a helicopter fly-over. There is no evidence of surface rupture along strike at the coast to the south (Clark et al., 2017), but differential lidar data do suggest the deformation extends to the north. The ruptures are primarily sinistral, with variable minor dip-slip components, and the maximum net displacement is estimated to be 1.8 (1.1–2.5) m (Table 2). An additional north-striking rupture has also been mapped between the Whites and Stone Jug faults from the lidar data (dashed red line on Fig. 1b). However, this rupture was not visible on a helicopter fly-over, corroborating the small vertical displacements measured

from the lidar data (≤0.2 m). Their presence highlights that we cannot discount the possibility of other small, diffuse, ruptures in this mountainous area.

Point Kean fault

A ~2.7-km-long, up-to-the-southeast, submarine rupture has been mapped east-northeast of the Kaikōura Peninsula, and has been named the Point Kean fault (Fig. 1b) (Clark et al., 2017). There was no prior surveying in this area, so it cannot be unequivocally stated that the scarp is entirely the result of the Kaikōura earthquake. No horizontal displacements have been identified, so the maximum net displacement of 2.6 (1.7–4) m is a dip-slip value only and should be considered a minimum. The length is also a minimum as the surveying was reconnaissance and other short traces cannot be discounted (Clark et al., 2017).

Kaikōura Peninsula fault

A submarine, northwest-dipping, reverse fault southeast of Kaikōura Peninsula (KPF on Fig. 1b) has long been inferred as a mechanism for uplift of flights of Holocene and Pleistocene marine terraces ringing and covering the Peninsula (Ota et al., 1996; Barrell, 2015; Litchfield et al., 2014, 2017), but no prior seismic surveying had been undertaken. Surveying following the Kaikōura earthquake also didn't identify a rupture there, but was of a reconnaissance nature as noted above, so short ruptures cannot be discounted. As mentioned earlier, Clark et al. (2017) proposed a fault source to account for the ~1 m uplift of Kaikōura Peninsula, which also fits with tsunami modelling. The source is a 38 km long, shallow, northwest-dipping, thrust fault (35° dip) with 3 m slip, that includes the Point Kean fault (Fig. 2).

Although not technically a surface rupture, but because it produced surface deformation, we have included the Kaikoura Peninsula fault in our 3D model (Fig. 5), and in the geological seismic moment and moment magnitude calculations with large length uncertainties (Table 3). The

Kaikōura Peninsula marine terrace record has been used to constrain a long-term (late Pleistocene) uplift rate of ~1.1 mm/yr (Ota et al., 1996), a recurrence interval of 900–1000 years (Barrell, 2015), and a most recent event prior to the Kaikoura earthquake of ~500 cal. yr BP (McFadgen, 1987; Litchfield et al., 2017) (Table 5).

Marlborough Fault System Surface Ruptures

Hope fault

A handful of short (≤0.2 km) ruptures occurred on the Conway and Seaward Segments of the Hope fault from approximately mid-way between the Conway-Charwell and Whites faults to the coast (Fig. 1b). No submarine ruptures were identified following re-surveying of the previously surveyed submarine traces (Clark et al., 2017). In the west (between the Stone Jug and Whites fault) the displacement was primarily vertical (<0.5 m). However, farther east the ruptures occur over a wider zone, where previous mapping (Eusden et al., 2000, 2005; Coulter, 2007; J. R. Pettinga, unpublished data) has documented a zone of partitioning between footwall *en echelon* fault wedges and dextral faults within the hanging-wall and into the lower parts of the mountain "escarpment". Displacement on the thrust wedges was ≤1 m and the dextral faults ≤1 m dextral and ≤0.4 m vertical. The maximum net displacement measured at one location on the Conway Segment is 1.1 (0.9–1.4) m (Table 2), but summing the displacements across the strands allows for a maximum net displacement of 1.5 (1–1.8) m. On the Seaward Segment at the coast the maximum displacement was 0.3 (0.2–0.5) m.

The Hope fault is one of the most active faults in New Zealand. Paleoseismic data exists for the Conway Segment, which has a slip rate of ≤23 ± 4 mm/yr, a recurrence interval of 180–310 years, and the most recent event prior to the Kaikōura earthquake was 230–110 cal. yr BP

(Langridge et al., 2003; Table 6). Single event displacement is 4–6 m (Pope, 1994; Manighetti et al., 2015). Values are inferred for the Seaward Segment (Table 6), but it is generally considered to be less active than the Conway Segment (e.g., slip rate 5 ± 1 mm/yr) as slip is partitioned northward onto the Jordan thrust (e.g., Van Dissen and Yeats, 1991); paleoseismic investigations on both segments are currently underway (e.g., Hatem et al., 2016).

Paparoa Point fault

Three short (≤0.4 km) northeast-striking, up-to-the-northwest ruptures crossing Paparoa Point ~1.6 km north of the Hope fault (Fig. 1b) were identified on differential lidar DEMs (Clark et al., 2017). They have not been surveyed in the field because of access issues when this portion of State Highway 1 was closed because of earthquake-triggered landslides. The displacements appear to be dextral-reverse (inferring a dip to the northwest), and the maximum displacement is 1.5 (0.8–2.3) m. This fault was not recognized prior to the Kaikōura earthquake, and so it was not included in the 2010 NSHM and there are no paleoseismic data.

Papatea fault

Approximately 19 km of rupture occurred along a series of north-northwest-striking faults or strands that we collectively refer to as the Papatea fault (Fig. 3c) (c.f. Langridge et al., 2018). These faults extend north from a point ~0.9 km north of the closest known trace of the submarine Seaward Segment of the Hope fault (~2.4 km east of the Paparoa Point fault), to the Jordan thrust and Kekerengu fault (Figs. 1b, 2, 5; Langridge et al., 2017, 2018). The strands have a range of senses of slip, but the Papatea fault is overall sinistral-reverse. The main Papatea fault dips moderately west and bounds the east side of a basement-cored range (Fig. 2). Displacement is also variable along its length (Fig. 4), but the maximum net displacement is 11.8 (10.4–13.9) m and the average displacement is 6.1 (4.3–6.9 m) (Table 2; Langridge et al., 2018). The $\%L½D_{max}$ is 70%

when calculated using the 15 km length for which displacements were measured (Fig. 4); it reduces to 55% if the full mapped length of 19 km is used.

The Papatea fault had been mapped as a major bedrock fault prior to the Kaikōura earthquake (Rattenbury et al., 2006), but evidence for its activity was equivocal (Barrell, 2015; Langridge et al., 2018), and so it was not included in the 2010 NSHM. The heights of fluvial terraces of inferred age above the modern riverbed have been used to infer a preliminary dip-slip rate of 1.7 ± 0.4 mm/yr, a recurrence interval of >5000–10,000 years, and 1–2 prior events within the Holocene (Langridge et al., 2018; Table 6). Paleoseismic studies of the Papatea fault are currently underway.

Upper Kowhai fault

Rupture occurred along ~13 km of the northeastern Upper Kowhai fault, from a prominent bend in the fault, to where it intersects the Jordan thrust (Figs. 1b, 2, 5; Kearse et al., 2018). The northeast-striking, moderately northwest-dipping fault, lies wholly within basement of the Seaward Kaikōura range (Fig. 2). The location within steep topography with few markers means there are no field displacement measurements, but the overall displacement appears to be dextral-normal, and a maximum net displacement is inferred from helicopter reconnaissance and lidar mapping to be 2.2 (1.4–3.1) m (Table 2).

The Upper Kowhai fault was known before the Kaikoura earthquake (Van Dissen 1989, 1991; Rattenbury et al., 2006; Barrell 2015), and is one of a series of faults between the Hope fault and the Kekerengu fault (Figs. 1b, 2). The Upper Kowhai fault was not explicitly included in the 2010 NSHM as it lies close to the Jordan thrust and was perceived as a potential secondary feature associated with the Jordan thrust rather than a fault source on its own (Stirling et al., 2012, 2017). There are no paleoseismic data available, so the slip rate of ~0.5 mm/yr, recurrence interval of

<2000 years, and the previous rupture event within the Holocene have all been inferred (Barrell, 2015; Table 6).

Manakau fault

Approximately 15 km of rupture occurred along the northeast-striking, southeast-dipping, Manakau fault, which is parallel to, and on the other side of the range crest from, the Upper Kowhai fault (Figs. 1b, 2; Kearse et al., 2018). Many "ridge rent" type features were also identified in the higher terrain, many of which are demonstrably related to gravitational extension and landslides, but other traces are of uncertain origin and may have contributed to distributed tectonic deformation. Like the Upper Kowhai fault, there are few displacement measurements along the Manakau fault, but the overall sense appears to be dextral-normal. Maximum displacement is inferred to be 1.5 (0.7–2.3) m (Table 2). The Manakau fault was not known prior to the Kaikōura earthquake and so was not included in the 2010 NSHM, and there are currently no paleoseimic data.

Jordan thrust

Rupture occurred along ~12 km of the northern part of the Jordan thrust, between the Upper Kowhai and Kekerengu faults (Figs. 1b, 2, 3e, 5; Kearse et al., 2018). The northeast-striking, northwest-dipping fault bounds and uplifts the southeast side of the Seaward Kaikōura range (Van Dissen and Yeats, 1991; Fig. 2), but the majority of the Kaikōura earthquake rupture was up-to-the-east. The central and northern parts (i.e., including the part that ruptured) of the Jordan thrust are entirely within basement rocks (Rattenbury et al., 2006; Fig. 2). Displacement was overall normal-dextral, and increased towards the northeast (e.g., Fig. 4), to a maximum of 7.5 (6.2–8.6) m (Table 2). The $\%L\frac{1}{2}D_{max}$ is 33%. An average displacement of 5.5 (4.5–6.5) m has been calculated

from a combined Upper Kowhai – Manakau – Jordan – Kekerengu – Needles net slip distribution, but much of the Jordan thrust rupture was smaller than that (Fig. 4; Kearse et al., 2018).

The Jordan thrust was well known prior to the Kaikōura earthquake (Van Dissen, 1989, 1991; Van Dissen and Yeats, 1991; Rattenbury et al., 2006; Barrell, 2015) although paleoseismic data are limited because of its steep mountainous location. It had been included in the 2010 NSHM as part of multi-fault sources with the Kekerengu and Needles faults, and the Kekerengu and Chancet faults (Stirling et al., 2012, 2017). The slip rate (primarily reverse, up-to-the-west) is inferred to be 20 ± 2 mm/yr (Robinson et al., 2011), the last event prior to the Kaikōura earthquake is <1730–1630 cal. yr BP from a faulted landslide deposit (Van Dissen et al., 2006; Table 6). A recurrence interval of 330 ± 70 years is calculated for the multi-fault sources in the 2010 NSHM (Stirling et al., 2012).

Fidget fault

East-northeast-striking ruptures have been mapped along ~5 km of the central Fidget fault, ~13 km west of its junction with the Jordan and Kekerengu faults (Figs. 1b, 2, 5). The fault dips steeply to the north and the ruptures cut basement rocks locally overlain by Quaternary fluvial deposits. There are few displacement measurements because of its remote location and lack of markers, but it appears to be overall normal-dextral, with a maximum of 1.5 (1.2–1.9) m (Table 2).

The Fidget fault was known prior to the Kaikōura earthquake (Van Dissen, 1989; Reay, 1993; Rattenbury et al., 2006; Barrell 2015), and has a total fault length of ~36 km. It had been included as a fault source in the 2010 NSHM (Stirling et al., 2012). There are no paleoseismology data, but a slip rate of 2 ± 1 mm/yr, and a last event prior to the Kaikōura earthquake in the

Holocene have been inferred (Table 6). A recurrence interval of $1185\ ^{+1425}_{-470}$ years was calculated for the 2010 NSHM (Stirling et al., 2012).

Kekerengu fault

The entire 26 km length of the northeast-striking Kekerengu fault ruptured, between the Jordan thrust in the southwest (which overlap for ~1.8 km) and the submarine Needles fault to the northeast (Figs. 1b, 2, 5; Kearse et al., 2018; Little et al., 2018). Overall, the rupture forms a relatively smooth broad arc (convex to the north) and dips steeply to the northwest, although local variations and complexities do occur (Kearse et al., 2018). The Kekerengu fault bounds basement-cored ranges to the northwest and Tertiary sediments to the southeast (Rattenbury et al., 2006) (Fig. 2). Displacements show some variability, but are overall reverse-dextral and large, the maximum being 11.9 (11.6–12.3) m and displacements along the entire length, except for the southern end where it overlaps the Jordan thrust, are greater than half the maximum (i.e., $\%L½D_{max}$ = 95%; Table 2; Kearse et al., 2018). As previously noted, the average displacement from the entire Upper Kowhai – Manakau – Jordan – Kekerengu – Needles slip distribution (Fig. 4) is 5.5 (4.5–6.5) m, but virtually all the Kekerengu fault displacements are larger than this.

The Kekerengu fault was well known prior to the Kaikōura earthquake (Van Dissen, 1989; Van Dissen et al., 2005; Rattenbury et al., 2006). A paleoseismic study was in fact underway and two of three trenches excavated 11 months prior to the earthquake were ruptured (Little et al., 2018). As noted for the Jordan thrust, the Kekerengu fault was included in the 2010 NSHM in two multi-fault sources (Stirling et al., 2012, 2017). The slip rate of 20–26 mm/yr is constrained from displacement optically stimulated luminescence (OSL) dated fluvial terraces (Van Dissen et al., 2016). The above-mentioned trenching study constrained the previous three earthquakes at 250–

110, 530–360, and 1250–900 cal. yr BP, and a recurrence interval of 380 ± 30 years (Table 2; Little et al., 2018).

Heaver's Creek fault

Rupture occurred along ~1.5 km of the Heaver's Creek fault, a northeast-striking, steeply southeast-dipping fault that is subparallel to, and considered a splay of, the Kekerengu fault (Fig. 1b; Kearse et al., 2018; Little et al., 2018). The total length of the Heaver's Creek fault is ~13 km and it lies within Miocene-Pliocene sediments with localized Quaternary fluvial deposits (Rattenbury et al., 2006; Fig. 2). There are only a few displacement measurements for this short rupture, but they are all pure dextral, and the maximum is 0.5 (0.2–0.8) m (Table 2). The Heaver's Creek fault was known prior to the Kaikōura earthquake, but was not included as an explicit fault source in the 2010 NSHM because of its close proximity to the Kekerengu fault (i.e., it was perceived as a potential secondary fault associated with the Kekerengu fault rather than a separate fault source).

Tinline Downs fault

Approximately 1.5 km of rupture occurred along a previously unknown fault north of the northeast end of the Kekerengu fault (Fig. 1b), named the Tinline Downs fault. The northeast-striking ruptures are scallop-shaped (convex to the east), and predominantly dextral, with an up-to-the-west dip-slip component. The maximum displacement is 1.5 (1.2–1.9) m.

The Tinline Downs fault bounds a prominent range-front and, cuts across Oligocene-Miocene sediments at a moderate angle (Fig. 2). Assuming the dip-slip component is reverse, we infer the fault dips to the west. As this fault was previously unknown it was not included in the 2010 NSHM and there is no paleoseismic information.

Needles fault

Rupture occurred along the southern 30–35 km of the northeast-striking Needles fault, from within ~0.8 km of where the Kekerengu fault runs offshore, to east of Cape Campbell in the vicinity of a releasing bend, and possibly at a small (180–440 m width) step-over about 10 km southwest of the Boo Boo fault intersection (Figs. 1b, 2, 5; Kearse et al., 2018). There are no markers to measure the horizontal component, but the overall displacement is inferred to be dextral-reverse, and is up-to-the-northwest along the southern half and mixed along the northern half (Kearse et al., 2018). The "maximum" displacement of 3.7 (3.0–4.9) m listed in Table 2 is therefore a dip-slip value only and is less than the average displacement of 5.5 (4.5–6.5) m for the entire Upper Kowhai – Manakau – Jordan – Kekerengu – Needles faults (noting, however, that the Needles fault portion is based on inferred slip distribution shapes).

The Needles fault was mapped prior to the Kaikōura earthquake (Barnes and Audru, 1999; Mountjoy et al., 2009; Wallace et al., 2012), but the 2016 rupture was 0.25–3 km landward of its previously mapped trace. It had been included in the 2010 NSHM as part of the Jordan-Kekerengu-Needles multi-fault source (Stirling et al., 2012, 2017). There are no paleoseismic data available, but a slip rate of 16 ± 2 mm/yr had been inferred (Robinson et al., 2011), as well as the previous event being within the Holocene (Table 6).

Needles SE fault

Approximately 0.9 km of rupture occurred on part (6–10%) of a northeast-striking thrust ~1 km southeast of the Needles fault (Fig. 1b; Kearse et al., 2018), here referred to as the Needles-SE fault. The rupture is up-to-the west and the "maximum" displacement is 1.8 (1.1–3.1) m (Table 2), but, like the other submarine faults, this is a dip-slip value only, and likely to be a minimum.

The Needles SE fault had not been previously identified, so it was not included in the 2010 NSHM, and there are no paleoseismic data.

Cape Campbell Road, Marfells Beach and Lighthouse faults

Short (<1 km) ruptures occurred on one previously known and two previously unknown faults on either side of the London Hill fault, the: Cape Campbell Road; Marfells Beach; and Lighthouse faults (Fig. 1b). The Marfells Beach fault is inferred to be reverse, although there are no markers to measure any horizontal displacement. The Cape Campbell Road and Lighthouse ruptures are dextral and reverse-dextral, respectively. The maximum displacements are all <1 m; 0.2 (0.1–0.3) m on the Cape Campbell Road fault, 0.3 (0.2–0.5) m on the Marfells Beach fault, and 0.8 (0.6–1.0) m on the Lighthouse fault.

The Cape Campbell Road fault had been previously mapped as an active fault – the last event was inferred to be within the Holocene (Van Dissen, 1995; Townsend and Little, 1998). These faults all lie within Miocene sediments (Fig. 2) and the Cape Campbell Road fault was interpreted to be a shallow seated, flexural slip fault in the Ward Syncline on the footwall of the London Hill fault. The Cape Campbell Road fault was not included in the 2010 NSHM, as it was assumed to be a secondary feature associated with the London Hill fault rather than a separate fault source.

Geological Seismic Moments and Moment Magnitudes

The calculated geological seismic moments and moment magnitudes for each fault, and the cumulative totals, are contained in Table 3. The mean seismic moments calculated using method 1 (D_{ave} for the 10 largest faults) for individual faults range from 1.60×10^{18} N m to 2.21×10^{20} N m and the mean moment magnitudes from M_w 6.1 to M_w 7.5, with the smallest being on the

Conway-Charwell fault and the largest being, not surprisingly, on the combined Upper Kowhai – Manakau – Jordan – Kekerengu – Needles faults. Using method 2 (NZ scaling relationships for all faults), the calculated mean seismic moments for individual faults range from 1.33×10^{15} N m to 2.35×10^{20} N m, and the mean moment magnitudes from M_w 4.1 to M_w 7.5, with the smallest and largest being on the Marfells Beach fault and the combined Upper Kowhai – Manakau – Jordan – Kekerengu – Needles faults, respectively.

The mean cumulative geological seismic moments (M_o^G) are 3.40×10^{20} ($1.79 \times 10^{20} – 7.55 \times 10^{20}$) N m using method 1, and 4.27×10^{20} ($2.25 \times 10^{20} – 9.65 \times 10^{20}$) N m using method 2 for the individual faults. These convert to geological moment magnitudes of M_w^G 7.7 ± 0.2, and M_w^G 7.7 (7.5–8.0), respectively. These calculated cumulative values entirely overlap within uncertainties. They also overlap, within uncertainties, the values derived from other, mostly geophysical, datasets (Table 1), as discussed in the next section.

Discussion

Role of the Hikurangi Subduction Interface in the Kaikōura Earthquake

Comparison of the cumulative geological seismic moment (M_o^G) and moment magnitudes (M_w^G) calculated from the surface rupturing faults (Table 3) with those from other datasets (Table 1), shows that the geological mean values are lower (M_o^G is 33–67% of those from other datasets), but the uncertainties generally overlap those from the other datasets, for which no uncertainties are given. However, as noted in the methods section, we propose that these values are minimum estimates for three main reasons. Firstly, Dolan and Haravitch (2014) present an analysis showing that on faults with a range of structural maturities subsurface displacement is a factor of 0.4–0.9

of the surface displacement. Secondly, as noted above, the geological history of the region and the analogue of the 1855 rupture on the Wairarapa fault that the current strike slip fault sole into listric structures resulting from prior tectonic evolution. Thirdly, well-located aftershocks of the Kaikōura earthquake extend to 25 km depth suggesting (in agreement with analysis of Wesnousky (2008) and Beeler at al. (2018)) that the Kaikōura rupture extended deeper in the crust than indicated by background seismicity occurring between large events. If we include these likely modifications to the M_o^G implied from surface displacement (Table 4) the resultant M_w^G is 7.8 ± 0.2, the same as the generally geophysically determined M_w of 7.8–7.9 (Table 1). There are significant uncertainties, but the differences are indicative of between 0 and 32% of the total moment on the subduction interface, or possibly a shallow dipping mid crustal detachment.

The complexity (multiple short faults at high angles to each other) of the surface rupture, which is difficult to resolve from seismological and other remote datasets, is undoubtedly a key reason why the full complexity of multi-fault rupture has not been included in several geophysically derived fault source models (Table 1). The Humps, Leader, Conway-Charwell, Hundalee, Whites, Point Kean, and Papatea, faults in particular, are all short (<30 km), have a complex geometry and meet each other at high angles. Other possible reasons that multiple fault sources have not been included in source models include that the some or all of fault planes identified as the subduction interface may in fact be mid crustal detachments, or a listric deep portion of the Kekerengu fault, an uncertainty acknowledged in some studies (e.g., Cesca et al., 2017; Hollingsworth et al., 2017; Wang et al., 2018).

Taken at face value, our 3D model (Fig. 5) suggests that most of the surface-rupturing faults do not physically connect with the subduction interface, and are up-dip of the area of the slip patch of Hamling et al. (2017) and Clark et al. (2017). However, as previously discussed, there is

uncertainty regarding the actual seismogenic depth in this part of New Zealand, and its base could be deeper than displayed in our model. The presence of a strong, cold slab that shallows to the east may also increase the depth to which rocks are brittle in the overlying greywacke crust (S. Ellis personal communication, 2017). The Vp = 6 km/s isosurface suggests considerable variability in the velocity structure at depth (Eberhart-Phillips and Bannister, 2010; Ellis et al., 2017; Figs. 4d, S1b), which could suggest variable seismogenic thickness across the crustal volume involved in the 2016 Kaikōura rupture. Therefore, the base of some faults (or sections of faults) may be relatively close (<5 km) to, or even in contact with, the subduction interface. We therefore consider the subduction interface, and/or possibly a mid crustal detachment, are probably important factors facilitating multi-fault rupture in the Kaikōura earthquake. The 3D model presented here, with consideration of the uncertainties on the seismogenic depth, alternative fault geometries (e.g., listric) and variation in crustal properties, could be used as a basis to reevaluate some of the published rupture models.

Other Factors Controlling Multi-Fault Ruptures and Absence of Major Rupture on the Hope Fault

Physical linkages between the crustal faults is another factor we consider important for facilitating rupture of multiple faults in the Kaikōura earthquake. The field mapping (Fig. 1b) and the 3D model (Figs. 5, S1) suggest that The Humps, Leader, Conway-Charwell, Stone Jug and Hundalee faults are physically connected – at the surface and most likely at depth – as are the Upper Kowhai, Manakau, Jordan, Papatea, Kekerengu, and Needles faults. Data are too sparse to rule out connections between the submarine part of the Hundalee fault and the Kaikōura Peninsula and Point Kean faults. This does raise the question, however, of why the Hope fault, one of the

most active faults in the area, and to which many of the faults likely connect at depth (Fig. 4), didn't undergo major (>1.5 m) surface displacement? That is, it did not sustain large seismic moment release similar as was observed on The Humps, Hundalee or Kekerengu faults (Holden et al, in 2017; Kaiser et al., 2017).

One possible reason that the Hope fault didn't undergo major rupture, at least at the surface, is that it was destressed by movement of faults and blocks on either side. Our 3D model suggests that the faults south of the Hope fault (The Humps to Point Kean/Kaikōura Peninsula faults) bound the south side of a crustal block that shifted eastwards relative to the Hope fault during the Kaikōura earthquake. This would have reduced shear stress on the dextral Hope fault and taken it further from failure. To the north of the Hope fault, the dextral component of motion on the Upper Kowhai fault and Jordan thrust would have similarly reduced shear stress on the Hope fault. Conversely, sinistral displacement on north- and north-northeast-striking faults such as the Leader, Stone Jug, Whites, and Papatea faults would have locally increased and decreased normal stress on the Hope fault at their points of intersection (i.e., the side pushing against the Hope Fault would have increased the normal stress, and vice versa), which could explain why there is deformation at only isolated locations along the Hope fault.

Regardless of whether the Hope fault ruptured at depth or not, the rupture clearly propagated from the less mature (i.e., the faults have accumulated less total displacement during the current tectonic regime), low slip rate faults in the NCD to the major through-going, high slip rate faults in the MFS, where displacements were highest. Thus, fault maturity is likely to be another factor for why multiple faults ruptured. That is, displacements were small and the ruptures more complex (multiple *en echelon* traces at a wide variety of orientations) on the faults in the

NCD, but were generally higher when the rupture reached the smoother, simpler Jordan-Kekerengu-Needles faults.

Another important factor controlling multi-fault ruptures may be crustal structure. In the near-surface, north-trending faults (e.g., the Leader and Stone Jug faults) appear to follow the pre-existing basement structural grain (with a dominant north-south orientation). These faults likely play an important role in connecting the major surface-rupturing faults (The Humps and Hundalee faults) with the Hope fault. At depth, highly variable crustal properties inferred from geophysical data (Eberhart-Phillips and Bannister, 2010) suggest abrupt changes in crustal properties such as elastic strength across some faults. This is demonstrated by plotting the Vp = 6 km/s isosurface (Ellis et al., 2017) as shown in Figs. 5d and S1b. Vertical steps in the isosurface of ≤10 km occur across parts of some of the faults in the region (e.g., >6 km depth difference across a part of the Hope fault and the Jordan thrust). Assuming that contrasts in Vp indicate changes in both elastic strength and other rheological parameters, then it follows that if such a volume of crust is under stress a complex deformation pattern may occur as deformation will be localized in areas of strength contrast (Ellis et al., 2017). It is perhaps relevant to note that the location of both the epicenter (near The Humps fault), and the location of maximum moment release (near the Kekerengu-Jordan-Fidget intersection) for the Kaikōura earthquake (e.g., Kaiser et al., 2017; Hamling et al., 2017; Holden et al., 2017) coincide with major changes in the Vp isosurface depth, and the presence of high velocity (presumably high strength) rocks at relatively shallow depths. The presence of the subduction slab, with its contrasting strength relative to overlying upper crustal rocks, adds even more complexity to the picture.

Some of the minor faults are likely to be secondary ruptures as a result of static or dynamic stress triggering from rupture of nearby major faults. We consider this to be likely for faults such

as the Paparoa Point fault near the Papatea fault, and the Heaver's Creek and Tinline Downs faults near the Kekerengu fault. The Lighthouse, Marfells Beach, and Cape Campbell Road faults could also be flexural-slip faults (Townsend and Little, 1998), similar to those that ruptured in the nearby 2013 Cook Strait earthquakes (Kaneko et al., 2015). The central Fidget fault rupture is more isolated (≥7 km from the closest rupture, the Jordan thrust), but is along-strike from the complex (Fidget-) Jordan-Kekerengu-Papatea fault junction (Langridge et al., 2017), is in the hanging-wall of the Jordan fault block, and is also near the modelled slip patch on the subduction interface (Figs. 5, S1). It has also been suggested that the Fidget fault ruptured in an aftershock (Ni, 2017), which warrants further investigation.

Implications for Seismic Hazard Modelling

The rupture of multiple faults in the Kaikōura earthquake clearly raises some challenges for fault source characterization in seismic hazard modelling, and reinforces the value of current attempts to incorporate or account for multi-fault ruptures (e.g., the UCERF3 approach – Field et al., 2014). Only about a third of the faults were included as fault sources in the 2010 NSHM (Table S1), and even after the event, it is still challenging to incorporate such a complex source in revisions of the NSHM fault source model. One important point to bear in mind, however, is that the Kaikōura earthquake was most likely a rare event. The earthquake ruptured faults with a wide range of slip rates and recurrence intervals (Tables 5 and 6), and in some cases only parts of faults, suggesting that the faults more typically rupture independently, or in different combinations. We estimate a recurrence interval of ≥5000-10,000 years for the Kaikōura earthquake (i.e., for repeat rupture involving all of the faults that ruptured in 2016), which is the average recurrence interval

for The Humps Fault, the lowest slip-rate surface-rupturing fault (Table 6). This estimate will be improved through ongoing paleoseismological investigations.

Another key lesson learnt is that the Kaikōura earthquake ruptured across a prominent tectonic domain boundary (the Hope fault), whereas in past seismic hazard models in New Zealand (e.g., the 2010 NSHM, Stirling et al., 2012) it was assumed that a fault rupture would not cross a domain boundary. Based on the previous sections discussion, we suggest that multi-fault rupture across tectonic domains should be considered in areas where there is: (1) the presence of a subduction interface (or a similar linking feature such as a mid-crustal detachment; e.g., Fletcher et al., 2014) in close proximity, but not necessarily in contact with, crustal faults, (2) a well-connected crustal fault network, (3) the presence of inherited basement structures at high angle to the major active faults, and/or (4) contrasts in crustal strength and thickness. It is important that, in addition to the earthquake geology data, the geological and structural history and 3D structure of a region is considered when characterizing fault sources for seismic hazard modelling.

Summary and Conclusions

Mapping of surface ruptures from the Kaikōura earthquake showed that over 20 faults with surface displacement of >0.5 m ruptured the ground surface or seafloor. The earthquake ruptured faults with a wide range of orientations, sense of movement, slip rates and recurrence intervals.

The maximum surface rupture displacement was ($11.9^{+0.4}_{-0.3}$ m) on the reverse-dextral Kekerengu fault, and the average displacement for the combined Upper Kowhai – Manakau – Jordan – Kekerengu – Needles faults is 5.5 ± 1 m. These faults are in the MFS, where ruptures are typically more continuous, linear, and larger than those in the NCD, and the rupture of the Kekerengu fault is the area of greatest seismic moment release. Similarly-large maximum (11.5 ±

2 m) and average (6.4 $^{+0.5}_{-1.2}$ m) surface rupture displacements occurred on the nearby, previously unrecognized, sinistral-reverse Papatea fault.

By contrast, surface ruptures were more complex in the NCD, consisting of short (≤3.4 km), *en echelon* and branching traces with mainly strike-slip or oblique reverse displacements. The maximum net displacement in the NCD was 5.5 $^{+1}_{-1.5}$ m on The Humps East fault, for which the average displacement was 1.5 $^{+0.2}_{-0.3}$ m.

Geological seismic moments ($M_o{}^G$) calculated from D_{ave} and New Zealand scaling relationships are 3.40×10^{20} ($1.79 \times 10^{20} – 7.55 \times 10^{20}$) N m and 4.27 x 10^{20} (2.25 x 10^{20} – 9.65 x 10^{20}) N m (individual faults), respectively. These convert to geological moment magnitudes of $M_w{}^G$ 7.7 ± 0.2 and $M_w{}^G$ 7.7 (7.5–8.0), but are all minimum values. A best estimate $M_w{}^G$ incorporating probable larger slip at depth by a factor of 1.4, a 20 km seismogenic depth, and likely listric geometry (average dip of 45°) is $M_w{}^G$ 7.8 ± 0.2. This interpretation suggests ≤32% of the seismic moment may be attributed the slip on the subduction interface. Alternatively, these increases to the $M_o{}^G$ as a result of shallowing fault dip with depth and larger slip at depth on these immature faults encompass the geophysically derived moment. This raises the possibility that rupture of shallow-dipping deeper parts of the surface faults (most notably the Kekerengu fault) has been mis-interpreted as subduction interface rupture.

The surface rupture mapping data and a 3D geological model suggest that likely factors contributing to the multi-fault rupture are: (1) the presence of a nearby, underlying, subduction interface or mid-crustal detachment; (2) physical linkages between faults; (3) rupture of geologically immature faults in the NCD; (4) inherited geological structure – both at shallow and greater depths, which results in contrasts in crustal strength and thickness; and (5) static or dynamic triggering of secondary faults, some of which may be flexural-slip faults. Some of these factors

may have facilitated that the Kaikōura earthquake ruptured across a tectonic domain boundary, which was not expected based on prior knowledge. Minor rupture of the Hope fault at only a few isolated locations may be the result of increased and decreased stress from rupture of faults on either side.

We estimate that the recurrence interval for the Kaikōura earthquake is ≥5000-10,000 years, at least a factor of ten longer than recurrence intervals of several of the high slip rate faults involved in the rupture. The Kaikōura earthquake is therefore a relatively rare event, and because it either wholly or partly ruptured faults with such a wide range of recurrence intervals, the faults more typically rupture independently, or in different combinations. Despite being rare cases, future seismic hazard models will need to incorporate complex ruptures (especially in settings or conditions such as 1 to 5 above) and multiple rupture scenarios, including the possibility of ruptures across different tectonic domains.

Data and Resources

The earthquake epicenters in Fig. 1b are from GeoNet (http://quakesearch.geonet.org.nz/) (Last accessed May 2018). A 1:250,000 scale map of the surface ruptures can be downloaded from the New Zealand active faults database (https://data.gns.cri.nz/af/, choose the Download Data – Kaikōura option) (last accessed May 2018). The 3D geological fault model was constructed using Seequent Leapfrog Geo (http://www.leapfrog3d.com/) (Last accessed May 2018). The remainder of datasets used come from published sources listed in the references.

Acknowledgments

Additional field assistance was given by Andrea Barrier, Alan Bischoff, Josh Borella, Rachel Carne, Matt Cockroft, Grace Duke, Fiona Fenton, Chris Grimshaw, Ken Hao, Marlene Villeneuve, Julian Thomson, and Anekant Wandres. Zoe Juniper is especially thanked for her logistical support. Susan Ellis helped in constructing the velocity isosurface shown in Figs. 4d and S1b, and contributed to discussions about crustal properties, as did Stephen Bannister. Caroline Holden is thanked for discussions about seismological aspects. We thank the landowners for unlimited access to their land and the crew and technicians on RV Tangaroa survey Tan1613, and RV Ikatere for marine surveying in difficult conditions. We are grateful for the support of Whalewatch Kaikōura. Funding was provided by GeoNet with the support of its sponsors New Zealand Earthquake Commission (EQC), GNS Science, and Land Information New Zealand, and Ministry of Business, Innovation and Employment (MBIE) response funding, provided through the Natural Hazards Research Platform (grant 2017-GNS-01-NHRP), and GNS Science MBIE strategic science investment funding (GNS-SSIF-TSZ). Funding for the offshore fault mapping work with RV Ikatere was provided by MBIE through the Natural Hazards Research Platform (grant C05X0907). The RV Tangaroa survey was funded by MBIE through the Endeavour Fund (grants C05X1605 and COPR1702) and the Tangaroa Reference Group. NSF-GEER Funding supported Hemphill-Haley, Madugo, Manousakis and Stahl, and Hatem and Zinke were funded by the Harry von Zell USC Geophysics Research Fund. Environment Canterbury, Land Information New Zealand, New Zealand Transport Authority, and AAM NZ Ltd are thanked for providing high quality lidar data. Reviews by Matt Hill, Tom Rockwell, James Dolan, and an anonymous reviewer resulted in many improvements to this article. We would also like to thank the Editors and the Editorial team for their help and patience.

References

Aki, K., and P. G. Richards (1980). *Quantitative Seismology: Theory and Methods,* W. H. Freeman, San Francisco, California.

Bai, Y., T. Lay, K. F. Cheung, and L. Ye (2017). Two regions of seafloor deformation generated the tsunami for the 13 November 2016, Kaikōura, New Zealand, earthquake, *Geophys. Res. Lett.* **44**, 6598-6606.

Barnes, P. M. (1996). Active folding of Pleistocene unconformities on the edge of the Australian-Pacific Plate boundary zone, offshore North Canterbury, New Zealand, *Tectonics* **15**, 623–640.

Barnes, P. M., and J. C. Audru (1999). Recognition of active strike-slip faulting from high-resolution marine seismic reflection profiles: Eastern Marlborough fault system, New Zealand, *Geol. Soc. Am. Bull.* **111**, 538-559.

Barrell, D. J. A. (2015). General distribuction and characteristics of active faults and folds in the Kaikōura District, North Canterbury, *GNS Science Consultancy Report* 2014/210 https://www.ecan.govt.nz/data/document-library/?ids=1645906,1811999,2147181,1811995,1512242,1242237,1394179,1337380,1059852,301544,1081016,2250897.

Barrell, D. J. A., and D. B. Townsend (2012). General distribution and characteristics of active faults and folds in the Hurunui District, North Canterbury, *GNS Science Consultancy Report* 2012/113, https://www.ecan.govt.nz/data/document-library/?ids=1645906,1811999,2147181,1811995,1512242,1242237,1394179,1337380,1059852,301544,1081016,2250897.

Bastin, S. H., M. Odgen, L. M. Wotherspoon, S. van Ballegooy, R. A. Green, M. Stringer, J. Stephenson, H. Edmiston, and C. Cappellaro (2018). Fluvial geomorphological influences on the distribution of liquefaction in the Wairau Plains, New Zealand following the 2016 Kaikōura Earthquake, *Bull. Seismol. Soc. Am.* **This volume**.

Beanland, S., K. R. Berryman, and G. H. Blick (1989). Geological invesitgations of the 1987 Edgecumbe earthquake, New Zealand, *New Zeal. J. Geol. Geophys.* **32**, 73-91.

Beavan, J., M. Motagh, E. J. Fielding, N. Donnely, N., and D. Collett (2012). Fault slip models of the 2010-2011 Canterbury, New Zealand, earthquakes from geodetic data and observations of postseismic ground deformation, *New Zeal. J. Geol. Geophys.* **55**, 207-221.

Beeler, N. M., G. Hirth, T. E. Tullis, and C. H. Webb (2018). On the depth of coseismic rupture, *Bull. Seismol. Soc. Am.* **108**, 761-780.

Bradley, B. A., Razafindrakoto, H. N. T., and V. Polak (2017). Ground-motion observations from the 14 November 2016 M_w 7.8 Kaikoura, New Zealand, earthquake and insights from broadband simulations, *Seis. Res. Lett.* **88**, 740-756.

Cesca, S., Y. Zhang, V. Mouslopoulou, R. Wang, J. Saul, M. Savage, S. Heimann, S. -K. Kufner, O. Oncken, and T. Dahm (2017). Complex rupture process of the Mw 7.8, 201k, Kaikoura earthquake, New Zealand and its aftershock sequence, *Earth Planet. Sci. Lett.* **478**, 110-120.

Clark, K., E. Nissen, J. Howarth, I. Hamling, J. Mountjoy, W. Ries, K. Jones, S. Goldstein, U. Cochran, P. Villamor, S. Hreinsdóttir, N. Litchfield, K. Berryman, and D. Strong (2017). Highly variable coastal deformation in the 2016 M_W7.8 Kaikōura earthquake reflects rupture complexity along a transpressional plate boundary, *Earth Planet. Sci. Lett.* **474**, 334-344.

Coulter, R. F. (2007) *Tectonic geomorphology and seismic hazard of the Mt Fyffe section of the Hope Fault,* MSc Thesis in Engineering Geology, University of Canterbury. 211 p.

Cowan, H. A., A. Nicol, and P. Tonkin (1996). A comparison of historical and paleoseismicity in a newly formed fault zone and a mature fault zone, North Canterbury, New Zealand, *J. Geophys. Res.* **101**, 6021–6036.

Dellow, S., Massey, C., Cox, S., Archibald, J. Begg, Z. Bruce, J. Carey, J. Davidson, F. Della Pasqua, P. Glassey, M. Hill, K. Jones, B. Lyndsell, B. Lukovic, S. McColl, M. Rattenbury, S. Read, B. Rosser, C. Singeisen, D. Townsend, P. Villamor, M. Villeneuve, J. Wartman, E. Rathjie, N. Sitar, A. -Z. Adda, J. Manousakis, and M. Little. (2017). Landslides caused by the Mw 7.8 Kaikōura Earthquake and the immediate response, *Bull. New Zeal. Soc. Earthquake Eng.* **50**, 106-116.

Dolan, J. F., and B. D. Haravitch (2014). How well do slip measurements track slip at depth in large strike-slip earthquakes? The importance of fault structural maturity in controlling on-fault slip versus off-fault surface deformation, *Earth Planet Sci. Lett.* **388**, 38-47.

Duputel, Z., and L. Rivera (2017). Long-period analysis of the 2016 Kaikōura earthquake, *Phys. Earth Planet. In.* **265**, 62-66.

Eberhart-Phillips, D., and S. Bannister (2010). 3-D imaging of Marlborough, New Zealand, subducted plate and strike-slip fault systems, *Geophys. J. Int.* **182**, 73-96.

Eberhart-Phillips, D., M. Reyners, S. Bannister, M.Chadwick, and S. Ellis (2010). Establishing a versatile 3-D seismic velocity model for New Zealand, *Seism. Res. Lett.* **81**, 992-1000.

Edbrooke, S. W., D. W. Heron, P. J. Forsyth, and R. Jongens, R. (compilers) (2015). Geological map of New Zealand 1:1 000 000, GNS Science, Lower Hutt. GNS Science Geological Map 2.

Ellis, S., R. Van Dissen, D. Eberhart-Phillips, M. Reyners, J. F. Dolan, and A. Nicol (2017). Detecting hazardous New Zealand faults at depth using seismic velocity gradients, *Earth Planet. Sci. Lett.* **463**, 333-343.

Eusden, J. D., J. R. Pettinga, and J. K. Campbell (2000). Structural evolution and landscape development of a collapsed transpressive duplex on the Hope Fault, North Canterbury, New Zealand, *New Zeal. J. Geol. Geophys.* **43**, 391-404.

Eusden, J. D., J. R. Pettinga, and J. K. Campbell (2005). Structural collapse of a transpressive hanging-wall fault wedge, Charwell region of the Hope Fault, South Island, New Zealand, *New Zeal. J. Geol. Geophys.* **48**, 295-309.

Field, E. H., R. J. Arrowsmith, G. P. Biasi, P. Bird, T. E. Dawson, K. R. Felzer, D. D. Jackson, K. M. Johnson, T. H. Jordan, C. Madden, A. J.Michael, K. R. Milner, M. T. Page, T. Parsons, P. M. Powers, B. E. Shaw, W. R. Thatcher, R. J. Weldon II, and Y. Zeng (2014). Uniform California Earthquake Rupture Forecast, Version 3 (UCERF3) - The Time-Independent Model, *Bull. Seismol. Soc. Am.* **104**, 1122-1180.

Fletcher, J. M., O. J. Teran, T. K. Rockwell, M. E. Oskin, K. W. Hudnut, K. J. Mueller, R. M. Spelz, S. O. Akciz, E. Masana, G. Faneros, E. J. Fielding, S. Leprince, A. E. Morelan, J. Stock, D. K. Lynch, A. J. Elliott, P. Gold, J. Liu-Zeng, A. González-Ortega1, A. Hinojosa-Corona1, and J. González-García1 (2014). Assembly of a large earthquake from a complex fault system: Surface rupture kinematics of the 4 April 2010 El Mayor-Cucapah (Mexico) M_w 7.2 earthquake, *Geosphere* **10**, 797-827.

Furlong, K. P., and M. Herman (2017). Reconciling the deformational dichotomy of the 2016 M_w 7.8 Kaikoura New Zealand earthquake, *Geophys. Res. Lett.* **44**, 6788-6791.

Goto, H., Tsutsumi, H., Toda, S., and Y. Kumahara (2017). Geomorphic features of surface ruptures associated with the 2016 Kumamoto earthquake in and around the downtown of Kumamoto City, and implications on triggered slip along active faults, *Earth Planets Space* **69**, 26, doi:10.1186/s40623-017-0603-9.

Grapes, R. H., and G. R. Holdgate (2014). Earthquake clustering and possible fault interactions across Cook Strait, New Zealand, during the 1848 and 1855 earthquakes, *New Zeal. J. Geol. Geophys.* **57**, 312-330.

Hamling, I. J., S. Hreinsdóttir, K. Clark, J. Elliott, C. Liang, E. Fielding, N. Litchfield, P. Villamor, L. Wallace, T. J. Wright, E. D'Anastasio, S. Bannister, D. Burbidge, P. Denys, P. Gentle, J. Howarth, C. Mueller, N. Palmer, C. Pearson, W. Power, P. Barnes, D. J. A. Barrell, R. Van Dissen, R. Langridge, T. Little, A. Nicol, J. Pettinga, J. Rowland, and M. Stirling (2017). Complex multi-fault rupture during the 2016 M_w 7.8 Kaikōura earthquake, New Zealand, *Science* **356,** no. 6334, eeam7194, doi: 10.1126/science.aam7194.

Hanks, T. C., and H. Kanamori (1979). A moment magnitude scale, *J. Geophys. Res.* **84**, 2348–2350.

Hatem, A. E., Dolan, J. F., Langridge, R. M., Zinke, R. W., McGuire, C. P., Rhodes, E. J., Van Dissen, R. J. (2016). Incremental slip rate and paleoseismic data from the eastern Hope fault, New Zealand: Hossack and Green Burn sites, *AGU Fall Meeting Abstracts*, abstract T32B-07.

Henrys, S., A.Wech, R. Sutherland, T. Stern, M. Savage, H. Sato, K. Mochizuki, T. Iwasaki, D. Okaya, A. Seward, B. Tozer, J. Townend, E. Kurashimo, T. Iidaka, and T. Ishiyama (2013). SAHKE geophysical transect reveals crustal and subduction zone structure at the southern Hikurangi margin, New Zealand, *Geochem. Geophys. Geosyst.* **14**, 2063-2083.

Holden, C., A. Kaiser, R. Van Dissen, and R. Jury (2013). Sources, ground motion and structural response characteristics in Wellington of the 2013 Cook Strait Earthquakes, *Bull. New Zeal. Soc. Earthquake Eng.* **46**, 188-195.

Holden, C., Y. Kaneko, E. D'Anastasio, R. Benites, B. Fry, and I. J. Hamling (2017). The 2016 M7.8 Kaikōura earthquake revealed by kinematic source inversion and seismic wavefield simulations: Slow rupture propagation on a geometrically complex crustal fault network, *Geophys. Res. Lett.* **44**, 11,320-11,328.

Hollingsworth, J., L. Ye, and J. -P. Avouac (2017). Dynamically triggered slip on a splay fault in the Mw 7.8, Kaikōura (New Zealand) earthquake, *Geophys. Res. Lett*. **44**, 3517-3525.

Kaiser, A., N. Balfour, B. Fry, C. Holden, N. Litchfield, M. Gerstenberger, E. D'Anastasio, N. Horspool, G. McVerry, J. Ristau, S. Bannister, A. Christophersen, K. Clark, W. Power, D. Rhoades, C. Massey, I. Hamling, L. Wallace, J. Mountjoy, Y. Kaneko, R. Benites, C. Van Houtte, S. Dellow, L. Wotherspoon, K. Elwood, and K. Gledhill (2017). The Kaikōura (New Zealand) Earthquake: Preliminary seismological report, *Seismol. Res. Lett.* **88**, 727-739.

Kaneko, Y., I. J. Hamling, R. J. Van Dissen, M. Motagh, and S. V. Samsonov (2015). InSAR imaging of displacement on flexural-slip faults triggered by the 2013 Mw 6.6 Lake Grassmere earthquake, central New Zealand, *Geophys. Res. Lett.* **42**, 781-788.

Kaneko, Y., E. Fukuyama, and I. J. Hamling (2017). Slip-weakening distance and energy budget inferred from near-fault ground deformation during the 2016 M_w 7.8 Kaikōura earthquake, *Geophys. Res. Lett.* **44**, 4765-4773.

Kearse, J., T. A. Little, R. J. Van Dissen, P. Barnes, R. Langridge, J. Mountjoy, W. Ries, P. Villamor, K. Clark, A. Benson, G. Lamarche, M. Hill, and M. Hemphill-Haley (2018)

Onshore to Offshore Ground-Surface and Seabed Rupture of the Jordan-Kekerengu-Needles Fault Network During the 2016, M_w 7.8 Kaikoura Earthquake, New Zealand, *Bull. Seismol. Soc. Am.* **This volume**, doi: 10.1785/0120170304.

Kurushin, R. A., A. Bayasgalan, M. Ölziybat, B. Enkhtuvshin, P. Molnar, C. Bayarsayhan, K. W. Hudnut, and J. Lin (1997). The surface rupture of the 1957 Gobi-Altay, Mongolia, earthquake, *Geol. Soc. Am. Spec. Pap.* **320**, 143 pp.

Langridge, R., J. Campbell, N. Hill, V. Pere, J. Pope, J. Pettinga, E. Estrada, and K. Berryman (2003). Paleoseismology and slip rate of the Conway Segment of the Hope Fault at Greenburn Stream, South Island, New Zealand, *Annals of Geophysics* **46**, 119-1139.

Langridge, R. M., W. F. Ries, N. J. Litchfield, P. Villamor, R. J. Van Dissen, D. J. A. Barrell, M. S. Rattenbury, D. W. Heron, S. Haubrook, D. B. Townsend, J. M. Lee, K. R. Berryman, A. Nicol, S. C. Cox, and M. W. Stirling (2016). The New Zealand Active Faults Database, *New Zeal. J. Geol. Geophys.* **59**, 86-96.

Langridge, R., W. Ries, J. Rowland, P. Villamor, J. Kearse, T. Little, E. Nissen, C. Madugo, N. Litchfield, C. Gasston, B. Hall, A. Canva, A. Hatem, and R. Zinke (2017). The role of surface-rupturing faults in the Waiautoa microblock, Clarence valley, New Zealand, during the M_w 7.8 2016 Kaikōura Earthquake. 8th International INQUA Meeting on Paleoseismology, Active Tectonics and Archeoseismology (PATA), 13-16 November, 2017, New Zealand. *GNS Science Misc. Ser.* **110**, 220-223.

Langridge, R.M., J. Rowland, P. Villamor, J. J. Mountjoy, C. Madugo, D. B. Townsend, W. R. Ries, K. J. Clark, T. A. Little, A. J. Canva, C. Gasston, B. Hall, A. Hatem, and A. Benson, (2018). Co-seismic rupture and slip on the Papatea fault and its role in the 2016 Kaikōura Earthquake, New Zealand, *Bull. Seismol. Soc. Am.* **This volume**.

Litchfield, N. J., J. K. Campbell, and A. Nicol (2003). Recognition of active reverse faults and folds in North Canterbury, New Zealand, using structural mapping and geomorphic analysis, *New Zeal. J. Geol. Geophys.* **46**, 563–579.

Litchfield, N. J., R. Van Dissen, R. Sutherland, P. M. Barnes, S. C. Cox, R. Norris, R. J. Beavan, R. Langridge, P. Villamor, K. Berryman, M. Stirling, A. Nicol, S. Nodder, G. Lamarche, D. J. A. Barrell, J. R. Pettinga, T. Little, N. Pondard, J. Mountjoy, and K. Clark (2013). A model of active faulting in New Zealand: fault zone parameter descriptions, *GNS Science Report* 2012/19. 109 p.

Litchfield, N. J., R. Van Dissen, R. Sutherland, P. M. Barnes, S. C. Cox, R. Norris, R. J. Beavan, R. Langridge, P. Villamor, K. Berryman, M. Stirling, A. Nicol, S. Nodder, G. Lamarche, D. J. A. Barrell, J. R. Pettinga, T. Little, N. Pondard, J. J. Mountjoy, and K. Clark (2014). A model of active faulting in New Zealand. *New Zeal. J. Geol. Geophys.* **56**, 32-56.

Litchfield, N. J., D. J. A. Barrell, A. Barrier, J. G. Begg, A. Benson, K. R. Berryman, A. Bischoff, K. J. Clark, U. A. Cochran, M. Cockroft, S. C. Cox, C. Fenton, C. Gasston, P. J. Glassey, D. Hale, B. Hall, A. Hatem, D. W. Heron, J. D. Howarth, Z. Juniper, N. Khajavi, J. Kearse, R. M. Langridge, S. Lawson, T. Little, B. Lukovic, S. McColl, A. Nicol, D. Noble, K. Pedley, J. Pettinga, W. Ries, J. Rowland, T. Stahl, M. W. Stirling, D. B. Townsend, V. Toy, P. Upton, A. Wandres, R. J. Van Dissen, P. Villamor, and R. Zinke (2016). 14th November 2016 M7.8 Kaikoura Earthquake. Preliminary surface fault displacement measurements. GNS Science. http://dx.doi.org/10.21420/G23W2R

Litchfield, N., K. Clark, T. Miyauchi, K. Berryman, D. Barrell, L. Brown, Y. Ota, and T. Fujimori (2017). Holocene marine terraces record long-term uplift along the Kaikōura coastline. 8th International INQUA Meeting on Paleoseismology, Active Tectonics and

Archeoseismology (PATA), 13-16 November, 2017, New Zealand, *GNS Science Misc. Ser.* **110**, 244-247.

Little, T. A. and A. Jones (1998). Seven million years of strike-slip and related off-fault deformation, northeastern Marlborough fault system, South Island, New Zealand, *Tectonics* **17**, 285-302.

Little, T. A., R. Grapes, R., and G. W. Berger (1998). Late Quaternary strike-slip on the eastern part of the Awatere fault, South Island, New Zealand, *Geol. Soc. Am. Bull.* **110**, 127-148.

Little, T. A., R. Van Dissen, J. Kearse, K. Norton, A. Benson, and N. Wang (2018). Kekerengu fault, New Zealand: timing and size of Late Holocene surface ruptures, *Bull. Seismol. Soc. Am.* **This volume**, doi:10.1785/0120170152.

McFadgen, B. G. (1987). Beach ridges, breakers and bones: late Holocene geology and archaeology of the Fyffe site, S49/46, Kaikoura Peninsula, New Zealand, *J. Roy. Soc. New Zeal.* **17**, 381-394.

Manighetti, I., C. Perrin, S. Dominguez, S. Garambois, Y. Gauhemer, J. Malavielle, L. Matteo, E. Delor, C. Vitard and S. Beupretre (2015). Recovering paleoearthquake slip record in a highly dynamic alluvial and tectonic region (Hope Fault, New Zealand) from airborne lidar, *J. Geophys. Res. Soild Earth* **120**, 4484-4509, doi:10.1002/2014JB01187.

Massey, C., D. Townsend, E. Rathje, K. Allstadt, Y. Kaneko, B. Lukovic, B. Bradley, J. Wartman, N. Horspool, I. Hamling, J. Carey, S. Cox, J. Davidson, S. Dellow, C. Holden, R. Jibson, K. Jones, A. Kaiser, M. Little, B. Lyndsell, S. McColl, R. Morgenstern, D. N. Petley, F. Rengers, D. Rhoades, B. Rosser, D. Strong, C. Singeisen, and M. Villeneuve (2018). Landslides triggered by the M_w 7.8 14 November 2016 Kaikoura Earthquake, New Zealand, New Zealand, *Bull. Seismol. Soc. Am.* **This volume**, doi: 10.1785/0120170305.

Matsuda, T. (1974). Surface faults associated with Nobi (Mino-Owari) Earthquake of 1891, Japan, *Bulletin of the Earthquake Research Institute, University of Tokyo* **13**, 127-162.

Meng, L., J. -P. Ampuero, Z. Duputel, Y. Luo, and V. C. Tsai (2012). Earthquake in a maze: compressional rupture branching during the 2012 M_w 8.6 Sumatra Earthquake, *Science* **337**, 724-726.

Mountjoy, J. J., P. M. Barnes, and J. R. Pettinga (2009). Morphostructure and evolution of submarine canyons across an active margin: Cook Strait sector of the Hikurangi Margin, New Zealand, *Mar. Geol.* **260**, 45-68.

Ni, S. (2017). Surface ruptures that could have been caused by aftershocks of the 2016 Kaikoura earthquake, Joint Scientific Assembly of the Inernational Association of Geodesy and the International Association of Seismology and Physics of the Earths Interior, Kobe, Japan, J02-3-02.

Nicol, A., and R. J. Van Dissen (2002). Up-dip partitioning of displacement components on the oblique-slip Clarence Fault, New Zealand, *J. Struct. Geol.* **24**, 1521–1535.

Nicol, A., B. Alloway, and P. Tonkin (1994). Rates of deformation, uplift and landscape development associated with active folding in the Waipara area of North Canterbury, New Zealand, *Tectonics* **13**, 1327–1344.

Nicol, A., H. Cowan, J. K. Campbell, and J. R. Pettinga (1995). Folding and the development of small sedimentary basins along the New Zealand plate boundary, *Tectonophysics* **241**, 47–54.

Nicol, A., N. Khajavi, J. Pettinga, C. Fenton, T. Stahl, S. Bannister, K. Pedley, N. Hyland-Brook, T. Bushell, I. Hamling, J. Ristau, S. Cox, D. Noble, and S. McColl, S. (2018). Preliminary geometry and kinematics of surface ruptures in the epicentral area during the 2016 M_W 7.8

Kaikōura earthquake, New Zealand, *Bull. Seismol. Soc. Am.* **This volume**, doi: 10.1785/0120170329.

Oskin, M. E., Arrowsmith, J. R., Corona, A. H., Elliott, A. J., Fletcher, J. M., Fielding, E. J., Gold, P. O., Gonzalez Garcia, J. J., Hudnut, K. W., Lio-Zeng, J., Teran, O. J. (2012). Near-field deformation from the El Mayor-Cucapah Earthquake revealed by differential LIDAR, *Science* **335**, 702-705.

Ota, Y., B. Pillans, K. Berryman, A. Beu, T. Fujimori, T. Miyauchi, and G. Berger (1996). Pleistocene coastal terraces of Kaikoura Peninsula and the Marlborough coast, South Island, New Zealand, *New Zeal. J. Geol. Geophys.* **39**, 51-73.

Pettinga, J. R., M. D. Yetton, R. J. Van Dissen, and G. Downes (2001). Earthquake source identification and characterisation for the Canterbury Region, South Island, New Zealand, *Bull. New Zeal. Soc. Earthquake Eng.* **34**, 282-317.

Pope, J. (1994). *Secondary structures, Holocene displacements and paleoseismicity of the Conway Segment of the Hope Fault, Greenburn Stream to Sawyers Creek.* Unpublished BSc. (Hons.) Project, Geological Sciences Library, University of Canterbury, Christchurch.

Power, W., K. Clark, D. King, J. Borrero, J. Howarth, E. Lane, D. Goring, J. Goff, C. Chague-Goff, J. Williams, C. Reid, C. Whittaker, C., Mueller, S. Williams, M. Hughes, J. Hoyle, J. Bind, D. Strong, N. Litchfield, and A. Benson (2017). Tsunami runup and tide-gauge observations from the 14 November 2016 M7.8 Kaikōura earthquake, New Zealand, *Pure App. Geophys.* **174**, 2457-2473.

Rattenbury, M. S., D. B. Townsend, and M. R. Johnston (2006). Geology of the Kaikōura area. Institute of Geological & Nuclear Sciences 1:250 000 geological map 13. 1 sheet + 70 p. Lower Hutt, New Zealand. GNS Science.

Reay, M. B. (1993). Geology of the middle part of the Clarence Valley. Lower Hutt: Institute of Geological & Nuclear Sciences. Institute of Geological & Nuclear Sciences geological map 10. 144 p. + 1 map

Reyners, M. (1998). Plate coupling and the hazard of large subduction thrust earthquakes at the Hikurangi subduction zone, New Zealand, *New Zeal. J. Geol. Geophys.* **41**, 343-354.

Reyners, M., D. Eberhart-Phillips, and S. Bannister (2017). Subducting an old subduction zone sideways provides insights into what controls plate coupling, *Earth Planet. Sci. Lett.* **466**, 53-61.

Robinson, R., R. Van Dissen, and N. Litchfield (2011). Using synthetic seismicity to evaluate seismic hazard in the Wellington region, New Zealand, *Geophys. J. Int.* **187**, 510-528.

Rodgers, D. W. and T. A. Little (2006). World's largest coseismic strike-slip offset: The 1855 rupture of the Wairarapa Fault, New Zealand, and implications for displacement/length scaling of continental earthquakes, *J. Geophys. Res.* **111**, B12408, doi:10.1029/2005JB004065.

Schwartz, D. P., P. J. Haeussler, G. G. Seitz, and T. E. Dawson (2012). Why the 2002 Denali fault rupture propagated onto the Totschunda fault: Implications for fault branching and seismic hazards, *J. Geophys. Res.* **117**, no. B11304, doi: 10.1029/2011JB008918.

Sieh, K., L. Jones, E. Hauksson, K. Hudnut, D. Eberhart-Phillips, T. Heaton, S. Hough, K. Hutton, H. Kanamori, A. Lije, S. Lindvall, S. F. McGill, J. Mori, C. Rubin, J. A. Spotila, J. Stock, H. K. Thio, J. Treiman, B. Wernicke, and J. Zachariasen (1993). Near-field investigations of the Landers Earthquake Sequence, April to July 1992, *Science* **260**, 171-176.

Stirling, M., M. Gerstenberger, N. Litchfield, G. McVerry, W. Smith, J. Pettinga, and P. Barnes, (2008). Seismic hazard of the Canterbury Region, New Zealand: new earthquake source model and methodology, *Bull. New Zeal. Soc. Earthquake Eng.* **41**, 51-65.

Stirling, M. W., G. McVerry, M. Gerstenberger, N. Litchfield, R. Van Dissen, K. Berryman, P. Barnes, L. Wallace, B. Bradley, P. Villamor, R. Langridge, G. Lamarche, S. Nodder, M. Reyners, D. Rhoades, W. Smith, A. Nicol, J. Pettinga, K. Clark, and K. Jacobs (2012). National seismic hazard model for New Zealand: 2010 update, *Bull. Seismol. Soc. Am.* **102**, 1514-1542.

Stirling, M. W., N. J. Litchfield, P. Villamor, R. J. Van Dissen, A. Nicol, J. Pettinga, P. Barnes, R. M. Langridge, T. Little, D. J. A. Barrell, J. Mountjoy, W. F. Ries, J. Rowland, C. Fenton, I. Hamling, C. Asher, A. Barrier, A. Benson, A. Bischoff, J. Borella, R. Carne, U. A. Cochran, M. Cockroft, S. C. Cox, G. Duke, F. Fenton, C. Gasston, C. Grimshaw, D. Hale, B. Hall, K. X. Hao, A. Hatem, M. Hemphill-Haley, D. W. Heron, J. Howarth, Z. Juniper, T. Kane, J. Kearse, N. Khajavi, G. Lamarche, S. Lawson, B. Lukovic, C. Madugo, I. Manousakis, S. McColl, D. Noble, K. Pedley, K. Sauer, T. Stahl, D. T. Strong, D. B. Townsend, M. Villeneuve, A. Wandres, J. Williams, S. Woelz, and R. Zinke (2017). The M_w 7.8 Kaikōura earthquake: Surface rupture, and seismic hazard context, *Bull. New Zeal. Soc. Earthquake Eng.* **50**, 73-84.

Stringer, M. E., S. Bastin, C. R. McGann, C. Cappellaro, M. E. Kortbawi, R. McMahon, L. W. Wotherspoon, R. A. Green, J. Aricheta, R. Davis, L. McGlynn, S. Hargraves, S. van Ballogooy, M. Cubrinovski, B. A. Bradley, X. Bellagamba, K. Forster, C. Lai, D. Ashfield, A. Baki, A. Zekkos, R. Lee, and N. Ntritsos (2017). Geotechnical aspects of the 2016

Kaikōura Earthquake on the South Island of New Zealand, *Bull. New Zeal. Soc. Earthquake Eng.* **50**, 117-141.

Townsend, D. B., and T. A. Little (1998). Pliocene-Quaternary deformation and mechanisms of near-surface strain close to the eastern tip of the Clarence Fault, northeast Marlborough, New Zealand, *New Zeal. J. Geol. Geophys.* **41**, 401-417.

Vanderleest, R. A., D. M. Fisher, D. O. S. Oakley, and T. W. Gardner (2017). Growth and seismic hazard of the Montserrat anticline in the North Canterbury fold and thrust belt, South Island, New Zealand, *J. Struct. Geol.* **101**, 1-14.

Van Dissen, R. J. (1989). *Late Quaternary faulting in the Kaikoura region, southeastern Marlborough, New Zealand*. Master of Science thesis, Oregon State University. 72 pp.

Van Dissen, R. J. (1991). An evaluation of seismic hazard in the Kaikoura region, southeastern Marlborough, *New Zeal. Geol. Surv. Rec.* **43**, 93-99.

Van Dissen, R. J. (1995). Immediate report: London Hill Fault. Institute of Geological and Nuclear Sciences, Lower Hutt. 9 p.

Van Dissen, R., and Y. S. Yeats (1991). Hope Fault, Jordan Thrust and uplift of the Seaward Kaikōura Range, New Zealand, *Geology* **9**, 393-396.

Van Dissen, R. J., K. Berryman, T. Webb, M. Stirling, P. Villamor, P. Wood, S. Nathan, A. Nicol, J. Begg, D. Barrell, R. McVerry, R. Langridge, N. Litchfield, and B. Pace (2003). An interim classification of New Zealand's active faults for the mitigation of surface rupture hazard, *Pacific Conference on Earthquake Engineering Paper* no.155.

Van Dissen, R. J., T. Little, and A. Nicol (2005). Field trip 4: faults of eastern Marlborough: Picton, Awatere and Kekerengu. In: Pettinga, J. R. and A. M. Wandres (eds) Geological

Society of New Zealand 50th annual conference, Kaikoura: field trip guides, *Geol. Soc. New Zeal. Misc. Publ.* **119B**, 85-110.

Van Dissen, R. J., D. G. Sutherland, R. J. Bowers, and J. L. Redwine (2006). Forest burial by large rock avalanche in Miller Stream, Seaward Kaikōura Range, New Zealand, c. 1700 years ago, *New Zeal. J. Geol. Geophys.* **49**, 151-157.

Van Dissen, R. J., T. A. Little, R. M. Burke, P. J. Tonkin, K. P. Norton, S. N. Bacon, R. Bowers, H. L. Goldstein, J. R. Redwine, D. G. Sutherland, S. F. Tillinghast, J. R. Kearse, J. Whattam, D. B. Townsend, A. M. Benson, and N. Wang (2016). Late Quaternary dextral slip rate of the Kekerengu Fault: New Zealand's third fastest on land fault, in Abstracts, GeoSciences 2016, Wanaka, Riesselman, C. and A. Roben (Editors), *Geosc. Soc. New Zeal. Misc. Pub.* 145A, p. 89.

Wallace, R. E. (1984). Fault scarps formed during the earthquakes of October 2 1915, Pleasant Valley, Nevada, and some tectonic implications, *U.S. Geol. Surv. Prof. Paper* 1274-A, B.

Wallace, L. M., J. Beavan, R. McCaffrey, K. Berryman, and P. Denys (2007). Balancing the plate motion budget in the South Island, New Zealand using GPS, geological and seismological data, *Geophys. J. Int.* **168**, 332–352.

Wallace, L. M., P. Barnes, J. Beavan, R. Van Dissen, N. Litchfield, J. Mountjoy, G. Lamarche, and N. Pondard (2012). The kinematics of a transition from subduction to strike-slip: an example from the central New Zealand plate boundary, *J. Geophys. Res.* **117,** no. B02405, doi: 10.1029/2011JB008640.

Wallace, L. M., S. Hreindsdottir, I. J. Hamling, E. D'Anastasio, and N. M. Barlow (2017a). Widespread afterslip and triggered slow slip events following the M7.8 Kaikoura earthquake, New Zealand, *AGU Fall Meeting Abstracts*, abstract G41A-08.

Wallace, L. M., Y. Kaneko, S. Hreindsdottir, I. Hamling, Z. Peng, N. Bartlow, E. D'Anastasio, and B. Fry (2017b). Large-scale dynamic triggering of shallow slow slip enhanced by overlying sedimentary wedge, *Nat. Geosci.* **10**, 765-772.

Wang, T., S. Wei, X. Shi, Q. Qiu, L. Li, D. Peng, R. J. Weldon, and S. Barbot (2018). The Kaikōura earthquake: Simultaneous rupture of the subduction interface and overlying faults, *Earth Planet. Sci. Lett.* **482**, 44-51.

Warren, G. (1995). Geology of the Parnassus area: sheets O32 & part N43, scale 1:50,000. Institute of Geological and Nuclear Sciences Geological Map 18.

Wen, Y. -Y., Ma, K. -F., Fry,B. (2018). Multiple-fault, slow rupture of the 2016 M_w 7.8 Kaikoura, New Zealand, Earthquake: Complementary insights from teleseismic and geodetic data, *Bull. Seismol. Soc. Am.* **This volume**, doi: 10.10785/0120170285.

Wesnousky, S. G. (2008). Displacement and geometrical characteristics of earthquake surface ruptures: issues and implications for seismic-hazard analysis and the process of earthquake rupture, *Bull. Seismol. Soc. Am.* **98**, 1609-1632.

Williams, C. A., D. Eberhart-Phillips, S. Bannister, D. H. N. Barker, S. Henrys, M. Reyners, and R. Sutherland (2013). Revised interface geometry for the Hikurangi Subduction Zone, New Zealand, *Seismol. Res. Lett.* **84**, 1066-1073.

Williams, J. N., D. J. A. Barrell, M. W. Stirling, K. M. Sauer, G. C. Duke, and K. X. Hao (2018). Surface rupture of the Hundalee Fault during the M_w 7.8 2016 Kaikōura Earthquake, *Bull. Seismol. Soc. Am.* **This volume**.

Yeats, R. S., and Berryman, K. R. (1987). South Island, New Zealand, and Transverse Ranges, California: A seismotectonic comparison, *Tectonics* **6**, 363-376.

Zhang, H., K. D. Koper, K. Pankow, and Z. Ge (2017). Imaging the 2016 M_w 7.8 Kaikōura, New Zealand, earthquake with teleseismic P waves: A cascading rupture across multiple faults, *Geophys. Res. Lett.* **44**, 4790-4798.

Zheng, A., M. Wang, X. Yu, and W. Zhang (2018). Source rupture process of the 2016 Kaikoura, New Zealand earthquake estimated from the kinematic waveform inversion of strong-motion data, *Geophys. J. Int.* **212**, 1736-1746.

Zinke, R., J. Hollingsworth, and J. F. Dolan (2014), Surface slip and off-fault deformation patterns in the 2013 Mw 7.7 Balochistan, Pakistan earthquake: Implications for controls on the distribution of near-surface coseismic slip, *Geochem., Geophys., Geosyst.* **15**, 5034-5050.

Author mailing list

GNS Science

PO Box 30-368

Lower Hutt 5040 New Zealand

(N.J.L., P.V., R.J.V., R.M.L., W.F.R., K.R.B., U.A.C., K.J.C., K.E.J., G.A., P.U., D.W.H., B.L., D.T.S., D.B.T.)

University of Canterbury

Private Bag 4800

Christchurch 8140 New Zealand

(A.N., J.R.P., C.F., N.K., D.H., D.N., K.P., T.S.)

National Institute of Water & Atmospheric Research

301 Evans Bay Parade

Wellington 6021 New Zealand

(P.M.B., J.J.M., T.J.K., G.L, S.W.)

GNS Science

Private Bag 1930

Dunedin 9054 New Zealand

(D.J.A.B., S.C.C.)

Victoria University of Wellington

PO Box 600

Wellington 6140 New Zealand

(T.A.L., J.K., A.B., J.H.)

The University of Auckland

Private Bag 92019

Auckland 1142 New Zealand

(J.R., C.G., B.H.)

University of Otago

PO Box 56

Dunedin 9054 New Zealand

(M.W.S., K.S., V.T., J.W.)

Humboldt State University

1 Harpst Street

Arcata CA 95521 U.S.A.

(M.H-H.)

GNS Science

Private Bag 2000

Taupo 3352 New Zealand

(C.A., S.L.)

University of Southern California

3651 Trousdale Parkway

Los Angeles CA 90089 U.S.A.

(A.E.H., R.Z.)

Physical Geography Group Massey University

Private Bag 11222

Palmerston North 4442 New Zealand

(S.T.M.)

Elxisgroup

Dimitressa 7-9

Athens 11528 Greece

(J. M.)

Pacific Gas and Electric Company

P.O. Box 997300

Sacramento, CA 95899-7300

(C.M)

Appendix

Discussion of Discrete Fault Definitions

One of the issues raised by the Kaikōura earthquake is definition/naming of discrete faults, and hence the total number of ground surface-rupturing faults described in this study. For the previously recognized active faults the names are generally based on previous definitions, which in turn are based on structural geology interpretations of faults being separated: (1) at branch points (e.g., Fidget to Kekerengu fault / Jordan thrust; Upper Kowhai fault to Jordan thrust); (2) by km-scale steps (e.g., Manukau and Upper Kowhai faults); and/or (3) if they have different senses of movement (e.g., Jordan thrust and Kekerengu faults) and/or slip rate (e.g., Heaver's Creek and Kekerengu faults). However, some of the names are a legacy of mapping by different past workers, such as the Kekerengu fault onshore and the Needles fault offshore; synchronous rupture of the Jordan-Kekerengu-Needles faults was identified as a likely scenario in the New Zealand National Seismic Hazard Model (Stirling et al., 2012, 2017).

Previously unrecognized faults are also generally distinguished on the basis of major changes in strike and sense of movement (e.g., the Stone Jug and Hundalee faults; the Papatea fault and Kekerengu fault / Jordan thrust); further work is needed to assess slip rates and paleoseismic evidence for synchronous rupture. Some of the previously unrecognized minor (<1.5 m maximum surface rupture displacement) surface ruptures are distinguished on the basis of differences in sense of movement, such as the along-strike Cape Campbell Road and Marfells Beach faults, which are dextral and reverse, respectively.

The above suggests that the total number of named faults (24) presented in this study is likely a maximum, and that further work may lead to faults being combined in the future. Conversely, however, the entire seafloor in the Kaikōura area has not been mapped and some lidar

data is still being processed, so we cannot rule out that there are additional surface ruptures, most likely minor (<1.5 m) displacement. This means that there is uncertainty in the total number of surface-rupturing faults, but we consider that the characteristics that we document neither change the geometric complexity of the rupture nor the first-order conclusions of the paper.

List of Figure Captions

Figure 1. (a) Tectonic setting with simplified active faults, tectonic domains, and cumulative net slip rates (Litchfield et al., 2014). The Pacific Plate motion vectors relative to the Australian Plate are from Wallace et al. (2007). ChCh = Christchurch, HT = Hikurangi Trough, MFS = Marlborough Fault System, NCD = North Canterbury Domain, Wgtn = Wellington. (b) Kaikōura earthquake surface ruptures, with their maximum displacements (in meters – circles mark the measurement locations – grid references are given in Table S1 in the electronic supplement to this article); cyan boxes = faults in the NSHM, grey boxes = faults not previously recognized as active, white boxes = remainder, blue numbers = slip rates (in mm/yr; Table 2). D = Downthrown side, f = fault, KPF = Kaikōura Peninsula fault (of Barrell, 2015), t = thrust, U = Upthrown side. A digital version of 2016 surface ruptures is available for download from the New Zealand Active Faults Database (Langridge et al. 2016). The basemap is from the NIWA bathymetry database.

Figure 2. Summary geological map of the Kaikōura earthquake surface rupture area, from Edbrook et al. (2015). The dashed line for the Kaikōura Peninsula fault marks the surface trace of the fault plane modelled by Clark et al. (2017). Black dots mark the intersection points of major fault ruptures. CCRF = Cape Campbell Road fault, f = fault, HCF = Heaver's Creek fault, LF = Lighthouse fault, MBF = Marfells Beach fault, NST = Needles – SE thrust, PKF = Point Kean fault, PPF = Paparoa Point fault, TDF = Tinline Downs fault.

Figure 3. (a) Sinistral-reverse ground surface rupture of the Leader fault, Woodchester Station, North Canterbury. Photograph taken by Kate Pedley. (b) Oblique-dextral surface rupture of the

Main Trunk Railway and State Highway 1 on the Hundalee fault, adjacent to where it runs offshore, and where the maximum displacement occurred. View to the north. Photograph taken by Julie Rowland. (c) Sinistral-reverse rupture of the Papatea fault across the Main Trunk Railway Line and State Highway 1 north of Waipapa Bay. View to the southwest. At the time of photography, a temporary one-lane access track had been constructed across the scarp. Photograph taken by Julian Thomson. (d) Terrestrial lidar, bathymetric lidar and multibeam hillshade model of the two strands of the Papatea fault crossing the coast. The resolution of the data is 1-2 m. (e) Normal-dextral rupture of the Jordan thrust across George Stream, a tributary to the Clarence River in the background. Photograph taken by Julie Rowland.

Figure 4. Net slip distributions for 10 of the major faults. The data are from Kearse et al. (2018) (Upper Kowhai – Needles faults), Langridge et al. (2018) (Papatea fault), Nicol et al. (2018) (The Humps, Leader, Conway-Charwell faults), and Williams et al. (2018) (Hundalee fault).

Figure 5. 3D geological model, showing simplified major faults in the area of the Kaikōura earthquake and the subduction interface after Williams et al. (2013). Note there are likely ±5 km uncertainties on the depths of all of these. (a) Oblique map view, towards the east. (b) Map view towards the north. (c) Cross section view towards the north. (d) Vp = 6 km/s coloured surface (Eberhart-Phillips et al., 2010; Ellis et al., 2017), also showing 1 km contours in the depth to this surface from a maximum of -6 to a minimum of -23 km. Figs. S1a and S1b in the electronic supplement to this article contains a 3D pdf of this model.

Table 1
Kaikōura earthquake fault source models

Reference	Data used	Number of rupturing faults	Faults[†]	M_w	M_o N m	Amount of M_o on the interface
Hollingsworth et al. (2017)	Optical satellite geodesy Teleseismic	2	Kek–Jord; Main thrust (subduction interface?)	-	-	60%
Zhang et al. (2017)	Teleseismic	2	Humps–Hund; Jord–Kek–Need	-	-	N/A
Bai et al. (2017)	Teleseismic Tide gauges	3	Humps–Hund; Subduction interface; Jord–Kek–Need	7.8	7.25×10^{20}	41%
Cesca et al. (2017)	Regional and teleseismic GPS InSAR	3	Humps–Lead–Hund; Deep thrust; Kek–Need	7.94	-	N/A
Wen et al. (2018)	Teleseismic, GPS	3	Humps–Lead–Hund; Kek-Need; Subduction interface	7.93	9.91×10^{20}	15–25%
Duputel and Rivera (2017)	Long-period seismology	3–4	Humps; Jord–Hope; Kek; Subduction interface	-	-	Significant[‡]
Kaiser et al. (2017)	Long-period seismology	4	Humps–Hund; ~Whites–UKowhai; Jord–Kek; Need	-	-	N/A
Wang et al. (2018)	Teleseismic, local strong ground motion GPS InSAR	11	Humps; Lead; Hund; SJug; Whites; UKowhai; Jord; Kek; Need; Pap Subduction interface	7.94	1.04×10^{21}	45%
Zheng et al. (2018)	Strong motion	13	~Humps; ~Lead (S and N); ~Con-Char; ~SJug; ~Hund; ~Whites; ~UKowhai; Jord; Kek; ~Fidget; ~Pap; ~Need	7.8	6.34×10^{20}	N/A
Hamling et al. (2017), updated by Clark et al. (2017)	Field - surface rupture Field - coastal uplift InSAR GPS Seismology	Multiple*	Humps; Lead; SJug; Hund; ~Whites; Hope; UKowhai–Jord– Kek–Need; LHill; Fidget; PKean/KPeninsula; ± Subduction interface	7.86	7.7×10^{20}	9%

*21 fault segments are modelled, but they correspond to 12 crustal faults as defined in this study.
†Faults preceded by an "~" are not named by the authors, and instead are our inferred correlations with faults on their source model maps. Faults preceded by a "±" indicates an additional fault in an alternative model. Con-Char = Conway-Charwell fault; Humps = The Humps fault; Hund = Hundalee fault; Jord = Jordan thrust; Kek = Kekerengu fault; KPeninsula = Kaikōura Peninsula fault; Lead = Leader fault; LHill = London Hill fault; N = North; Need = Needles fault; Pap = Papatea fault; PKean = Point Kean fault; S = South; SJug = Stone Jug fault; UKowhai = Upper Kowhai fault.

‡ M_o is not given, but the magnitude on the four segments are Humps M_w 7.2; Jord–Hope M_w 7.4; Kek M_w 7.6; Subduction interface M_w 7.6.

Table 2
Kaikōura earthquake surface rupture data

Fault name[*]	Mapped Length (*L*) (km)	Sense[†]	Inferred[‡] fault dip (°)	Dip Dir.[§]	Horizontal D_{max}‖ (m)	Vertical D_{max}‖ (m)	Net D_{max}‖,[1] (m)	%L½D_{max}[3]	Net D_{ave}[5] (m)
Lighthouse	1	Rev-Dex	70 ± 10	W	0.6 ± 0.1	0.5 ± 0.1	0.8 (0.6–1.0)		
Marfells Beach	<1	Reverse	70 ± 10	W	0	0.3 ± 0.1	0.3 (0.2–0.5)		
Cape Campbell Road	<1	Dextral	65 ± 10	W	0.2 ± 0.1	0	0.2 (0.1–0.3)		
Needles	**34**	**Dex-Rev**	**70 ± 15**	**NW**	**unknown**	**3.5 ± 0.5**	**≥3.7 (3.0–4.9)**[2]		**5.5 (4.5–6.5)**[6]
Needles – SE thrust	**0.9**	**Dextral**	**55 ± 15**	**SE**	**unknown**	**1.5 ± 0.5**	**≥1.8 (1.1–3.1)**[2]		
Tinline Downs	1.5	DS-Dex	50 ± 20	W	1.5 ± 0.3	0.1 ± 0.2	1.5 (1.2–1.9)		
Kekerengu	**26**	**Rev-Dex**	**70 ± 10**	**NW**	**11.8 ± 0.3**	**1.8 ± 0.2**	**11.9 (11.6–12.3)**	**95%**	**5.5 (4.5–6.5)**[6]
Heaver's Creek	1.5	Dextral	80 ± 10	SE	0.5 ± 0.3	0	0.5 (0.2–0.8)		
Fidget	5	Nor-Dex	70 ± 10	N	1.5 ± 0.3	0.3 ± 0.1	1.5 (1.2–1.9)		
Jordan thrust	**12**	**Nor-Dex**	**50 ± 10**	**NW**	**7.0 ± 1.0**	**2.0 ± 0.5**	**7.5 (6.2–8.6)**	**33%**	**5.5 (4.5–6.5)**[6]
Manakau	15	Dex-Nor	70 ± 10	SE	1.0 ± 0.5	1.0 ± 0.5	1.5 (0.7–2.3)		**5.5 (4.5–6.5)**[6]
Upper Kowhai	**13**	**Dex-Nor**	**70 ± 10**	**NW**	**1.5 ± 0.5**	**1.5 ± 0.5**	**2.2 (1.4–3.1)**		**5.5 (4.5–6.5)**[6]
Papatea	**19**	**Sin-Rev**	**55 ± 10**	**W**	**4.3 ± 0.5**	**9.0 ± 0.2**	**11.8 (10.4–13.9)**	**70%**	**6.1 (4.3–6.9)**
Paparoa Point	<1	Dex-Rev	70 ± 10	NW	0.7 ± 0.4	1.2 ± 0.5	1.5 (0.8–2.3)		
Hope Seaward	<1	Dex-Rev	70 ± 10	NW	0.1 ± 0.05	0.3 ± 0.1	0.3 (0.2–0.5)		
Hope Conway	>1	Rev-Dex	70 ± 10	NW	1.0 ± 0.2	0.5 ± 0.2	1.1 (0.9–1.4)		
Point Kean	**2.7**	**Rev-SS**	**55 ± 15**	**NW**	**unknown**	**2.1 ± 0.5**	**≥2.6 (1.7–4.0)**[2]		
Whites	**4**	**DS-Sin**	**90 ± 10**		**1.5 ± 0.5**	**1.0 ± 0.5**	**1.8 (1.1–2.5)**		
Hundalee	**23**	**DS-Dex**	**85 ± 5**	**NW**	**3.7 ± 0.5**	**1.5 ± 0.5**	**4.0 (3.4–4.7)**	**17%**	**1.2 (0.9–2.7)**
Stone Jug	19	DS-Sin	85 ± 5		0.7 ± 0.1	0.3 ± 0.1	0.8 (0.6–0.9)		
Conway - Charwell	**5**	**Dex-Rev**	**80 ± 10**	**NW**	**0.5 ± 0.2**	**1.5 ± 0.2**	**1.6 (1.3–1.9)**	**32%**	**0.7 (0.5–0.9)**
Leader	**28**	**Sin-Rev**	**80 ± 10**	**E**	**2.2 ± 0.15**	**3.3 ± 0.5**	**4.0 (3.5–4.7)**	**6%**	**1.2 (1.0–1.5)**
The Humps West	**20**	**Rev-Dex**	**75 ± 10**	**S**	**3.9 ± 0.4**	**0.5 ± 0.2**	**3.9 (3.5–4.4)**	**21%**[4]	**1.5 (1.2–1.7)**[4]
The Humps East	**16**	**Dex-Rev**	**60 ± 10**	**NW**	**0.5 ± 0.5**	**3.5 ± 0.5**	**4.1 (3.2–5.3)**	**21%**[4]	**1.5 (1.2–1.7)**[4]

[*]The names follow previous definitions or are newly named in this study as discussed in the Appendix. They are ordered north to south, and faults in bold are those with major (>1.5 m) maximum net surface rupture displacement.

[†]Sense of movement in the Kaikōura earthquake, expressed as secondary-dominant. Dex = dextral, DS = Dip-slip, Nor = Normal, Rev = reverse, Sin = Sinistral, SS = Strike-slip.

[‡]Inferred average or representative dip.

[§]Dir = direction.

‖D_{max} = maximum surface rupture displacement. Grid references for these locations are contained in Table S1 in the electronic supplement to this article.

[1]values in brackets are minimum and maximum values, considered to represent a 95% confidence interval.

[2] Dip-slip displacement only; net displacement is likely to be larger.

[3]Percentage of the fault length with displacements greater than half of the maximum displacement.

[4]Calculated for all of The Humps fault (i.e., combined West and East sections).

[5]D_{ave} = average surface rupture displacement, calculated from the area under the net slip curve divided by length.

[6]Combined average displacement for the Needles – Kekerengu – Jordan – Manakau – Upper Kowhai faults.

Table 3
Calculated (minimum) geological seismic moment and moment magnitude estimates

Fault name	Length (L) (km)	Net D_{ave} (m)	Method 1 - D_{ave}		Method 2 – NZ M_w-Length scaling relationship	
			M_o^G N m	M_w^G	M_w^G	M_o^G N m
Lighthouse	0.2 (0.2–1)				5.0 (4.8–5.1)	3.34×10^{16} (2.06×10^{16}–5.84×10^{16})
Marfells Beach	1 (0.9–1)				4.1 (3.9–5.1)	1.33×10^{15} (8.24×10^{14} –4.83×10^{16})
Cape Campbell Road	0.3 (0.3–1)				4.2 (4.2–5.1)	3.11×10^{15} (1.89×10^{15}–5.10×10^{16})
Needles	**34 (30–35)**					
Needles – SE thrust	**0.9 (0.8–1)**				**5.0 (4.8–5.2)**	**3.10×10^{16} (1.81×10^{16}–6.50×10^{16})**
Tinline Downs	1.5 (1.4–2)				5.3 (5.1–5.4)	9.20×10^{16} (4.86×10^{16}–2.28×10^{17})
Kekerengu	**26 (23–29)**					
Heaver's Creek	1.5 (1.4–2)				5.2 (5.1–5.4)	7.16×10^{16} (4.57×10^{16}–1.21×10^{27})
Fidget	5 (4–14)				5.9 (5.7–6.6)	8.34×10^{17} (4.07×10^{17}–9.46×10^{18})
Jordan thrust	**12 (11–15)**					
Manakau	15 (12–17)					
Upper Kowhai	**13 (9–17)**					
Needles-U. Kowhai*	**84 (76–92)**	**5.5 (4.5–6.5)**	**2.21×10^{20} (1.24×10^{20}–5.10×10^{20})†**	**7.5 (7.4–7.8)**	**7.5 (7.4-7.8)**	**2.35×10^{20} (1.46×10^{20}-5.05×10^{20})**
Papatea	**19 (18–20)**	**6.1 (4.3–6.9)**	**6.37×10^{19} (2.56×10^{19}–1.17×10^{20})**	**7.2 (6.9–7.3)**	**6.7 (6.5–6.9)**	**1.38×10^{19} (6.22×10^{18}–2.36×10^{19})**
Paparoa Point	0.6 (0.5–1)				4.7 (4.5–5.1)	1.20×10^{16} (7.42×10^{15}–4.83×10^{16})
Hope Seaward	0.3 (0.3–1)				4.3 (4.1–5.1)	3.00×10^{15} (1.86×10^{15}–4.83×10^{16})
Hope Conway	1.5 (1–2)				5.2 (5.6–6.5)	7.50×10^{16} (2.54×10^{16}–1.31×10^{17})
Pt Kean/Kaikoura P	**38 (20–50)**				**7.2 (6.7–7.6)‡**	**7.89×10^{19} (1.41×10^{19}–2.47×10^{20})**
Whites	**4 (3.6–13)**				**5.8 (5.6–6.5)**	**5.01×10^{17} (3.25×10^{17} –7.17×10^{18})**
Hundalee	**23 (14–31)**	**1.2 (0.9–2.7)**	**1.25×10^{19} (4.54×10^{18}–5.10×10^{19})**	**6.7 (6.4–7.1)**	**6.8 (6.3–7.0)**	**1.66×10^{19} (3.61×10^{18}–4.08×10^{19})**
Stone Jug	19 (18–21)				6.7 (6.6–6.8)	1.14×10^{19} (8.12×10^{18}–1.85×10^{19})
Conway - Charwell	**5 (4–6)**	**0.7 (0.5–0.9)**	**1.60×10^{18} (7.20×10^{17}–3.45×10^{18})**	**6.1 (5.9–6.3)**	**6.1 (6.8–7.1)**	**7.96×10^{17} (4.01×10^{17}–1.60×10^{18})**
Leader	**28 (25–32)**	**1.2 (1.0–1.5)**	**1.54×10^{19} (9.0×10^{18}–3.06×10^{18})**	**6.8 (6.6–7.0)**	**6.9 (6.8–7.1)**	**2.49×10^{19} (1.57×10^{19}–4.55×10^{19})**
The Humps W&E	**36 (34–37)**	**1.5 (1.2–1.7)**	**2.58×10^{19} (1.49×10^{19}–4.36×10^{19})§**	**6.9 (6.7–7.1)**	**7.1 (6.9–7.2)**	**4.32×10^{19} (2.94×10^{19}–6.61×10^{19})**
TOTALS			**3.40×10^{20} (1.79×10^{20}–7.55×10^{20})**	**7.7 (7.5–7.9)**	**7.7 (7.5–8.0)**	**4.27×10^{20} (2.25×10^{20}–9.65×10^{20})**

*Combined Needles, Kekerengu, Jordan thrust, Manakau, and Upper Kowhai faults.
†Calculated using a dip of 70° (45°–80°).
‡Calculated using a dip of 35° (25°–45°).
§Calculated using a dip of 70° (60°–80°).

Table 4
Alternative cumulative geological moment magnitude and seismic moment calculations

Alternative calculations	Methods	M_w^G	M_o^G N m	% of M_o from other datasets (Table 1)
Original	1	7.7 (7.5–7.9)	3.4×10^{20} (1.8×10^{20}–7.6×10^{20})	33–54
	2	7.7 (7.5–8.0)	4.3×10^{20} (2.3×10^{20}–9.7×10^{20})	41–67
SSR* = 0.7	1	7.8 (7.6–8.0)	4.8×10^{20} (2.5×10^{20}–1.0×10^{21})	46–75
Depth = 20 km	1	7.7 (7.6–7.9)	4.5×10^{20} (2.7×10^{20}–8.3×10^{20})	44–72
	2	7.7 (7.7–8.0)	5.7×10^{20} (3.4×10^{20}–1.1×10^{21})	55–90
SSR = 0.7, Depth = 20 km	1	7.8 (7.7–8.0)	6.4×10^{20} (3.8×10^{20}–1.2×10^{21})	61–100
	2	7.8 (7.7–8.0)	5.7×10^{20} (3.4×10^{20}–1.1×10^{21})	54–90
Dip = 45°	1	7.7 (7.5–8.0)	4.4×10^{20} (2.1×10^{20}–9.8×10^{20})	43–70
	2	7.8 (7.6–8.0)	5.3×10^{20} (2.7×10^{20}–1.1×10^{21})	51–83
All	1	7.9 (7.7–8.1)	7.7×10^{20} (4.2×10^{20}–1.4×10^{21})	74–121
	2	7.9 (7.7–8.0)	7.0×10^{20} (4.0×10^{20}–1.3×10^{21})	68–111

*SSR = ratio of sub surface to surface displacement (D_{ave}), or sub surface displacement is 1.4× surface displacement. It only affects values calculated using method 1.

Table 5
Previous (paleoseismic) surface rupture data and estimates for the NCD faults

Fault name	Sense of displacement		Slip rate (mm/yr)	Recurrence interval (years)	Event prior to the Kaikōura Earthquake (cal. yr BP)
	Predominant	Subordinate			
Point Kean	-		-	-	-
Kaikōura Peninsula	Reverse	-	1.1 (uplift rate) Barrell (2015)	~900–1000 Barrell (2015)	~500 McFadgen (1987)
Whites	-		-	-	
Hundalee	Reverse	Dextral	$1.2\ ^{+1.2*}_{-0.8}$ Litchfield et al. (2013, 2014)	$3080\ ^{+7075*}_{-1630}$ Stirling et al. (2012)	<11800–>110[†]
Stone Jug	-		0.05–2[*] Barrell and Townsend (2012)	≥6000[*] Barrell and Townsend (2012)	<11800–>110[†]
Conway - Charwell	Dextral	Reverse	0.05–2[*] Barrell and Townsend (2012)	≥6000[*]	<11800–>110[†]
Leader	-		-	-	-
The Humps (West and East)	Reverse		0.2 ± 0.1[*] Barrell and Townsend (2012)	5000-10,000[†]	<11800–>110[†]

[*]Calculated from some field observations and inferences (e.g., age of geomorphic surface, magnitude-scaling relationships).
[†]Inferred taking into account some field observations (e.g., scarp height and freshness).

Table 6
Previous (paleoseismic) surface rupture data and estimates for the MFS Domain faults

Fault name	Sense of displacement		Slip rate (mm/yr)	Recurrence interval (years)	Event prior to the Kaikōura Earthquake (cal. yr BP)
	Predominant	Subordinate			
Marfells Beach	-		-	-	-
Lighthouse	-		-	-	-
Cape Campbell Road	Reverse Townsend and Little (1998)		-	-	<11800 - >110*
Needles	Dextral	Reverse	16 ± 3* Robinson et al. (2011)	-	<11800 - >110*
Needles – SE thrust	Reverse		-	-	-
Tinline Downs	-		-	-	-
Kekerengu	Dextral	Reverse	20–26† Van Dissen et al. (2016)	380 ± 30† Little et al. (2018)	250–110† Little et al. (2018)
Heaver's Creek	Dextral	Reverse	≤0.8‡ Barrell (2015)	~2400–6000† Barrell (2015)	<11800–>110* Langridge et al. (2016)
Fidget	Dextral		2 ± 1* Litchfield et al. (2014)	$1185\ ^{+1425}_{-470}$§ Stirling et al. (2012)	<11800–>110*
Papatea	Reverse	Sinistral	1.7 ± 0.4 (dip slip)§ Langridge et al. (2018)	>5000-10,000§ Langridge et al. (2018)	<11800–>110§ Langridge et al. (2018)
Jordan thrust	Reverse	Dextral	20 ± 2*,‖ Robinson et al. (2011)	330 ± 70‡ Stirling et al. (2012)	<1730-1630 Van Dissen et al. (2006)
Manakau	-		-	-	-
Upper Kowhai	Reverse		~0.5§ Barrell (2015)	<2000* Van Dissen et al. (2003)	<11800–>110* Langridge et al. (2016)
Paparoa Point	-		-	-	-
Hope Seaward	Dextral		5 ± 1* Robinson et al. (2011)	$720\ ^{+355}_{-230}$‡ Stirling et al. (2012)	<5000*
Hope Conway	Dextral		≤23 ± 4† Langridge et al. (2003)	180–310† Langridge et al. (2003)	230–110† Langridge et al. (2003)

*Inferred taking into account some field observations (e.g., scarp height and freshness, inferred age of displaced markers).
†From field-based paleoseismic data.
‡Calculated by combining two values which in turn were calculated as explained in footnote §.
§Calculated from some field observations and inferences (e.g., age of geomorphic surface, magnitude-scaling relationships).

‖Most of this slip rate is considered to be accommodated on blind faulting and folding (Van Dissen and Yeats, 1991).

Figure 1

Click here to download Figure Fig1-FaultMap.tif

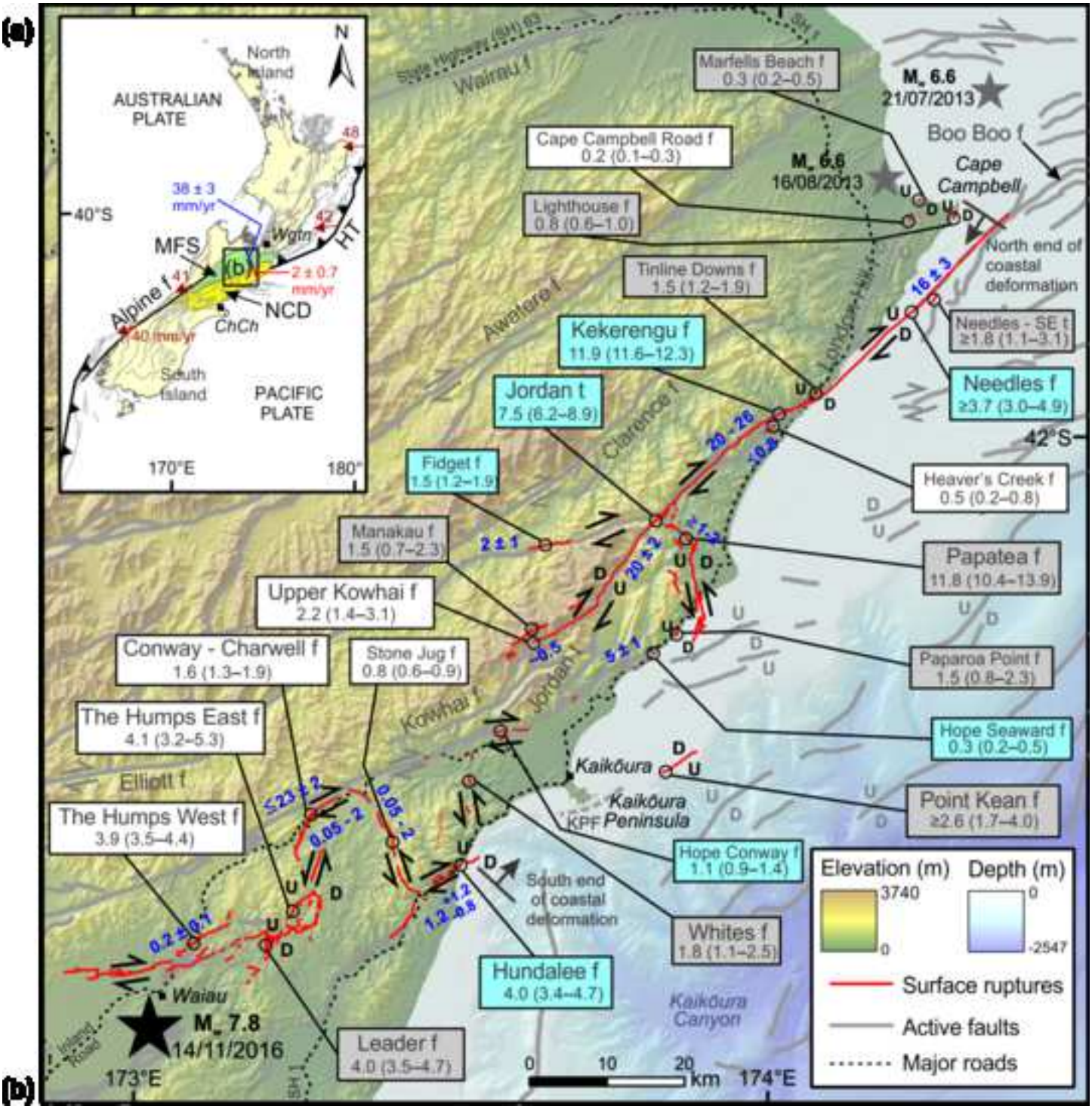

Figure 2

Click here to download Figure Fig2-GeologyMap.tif

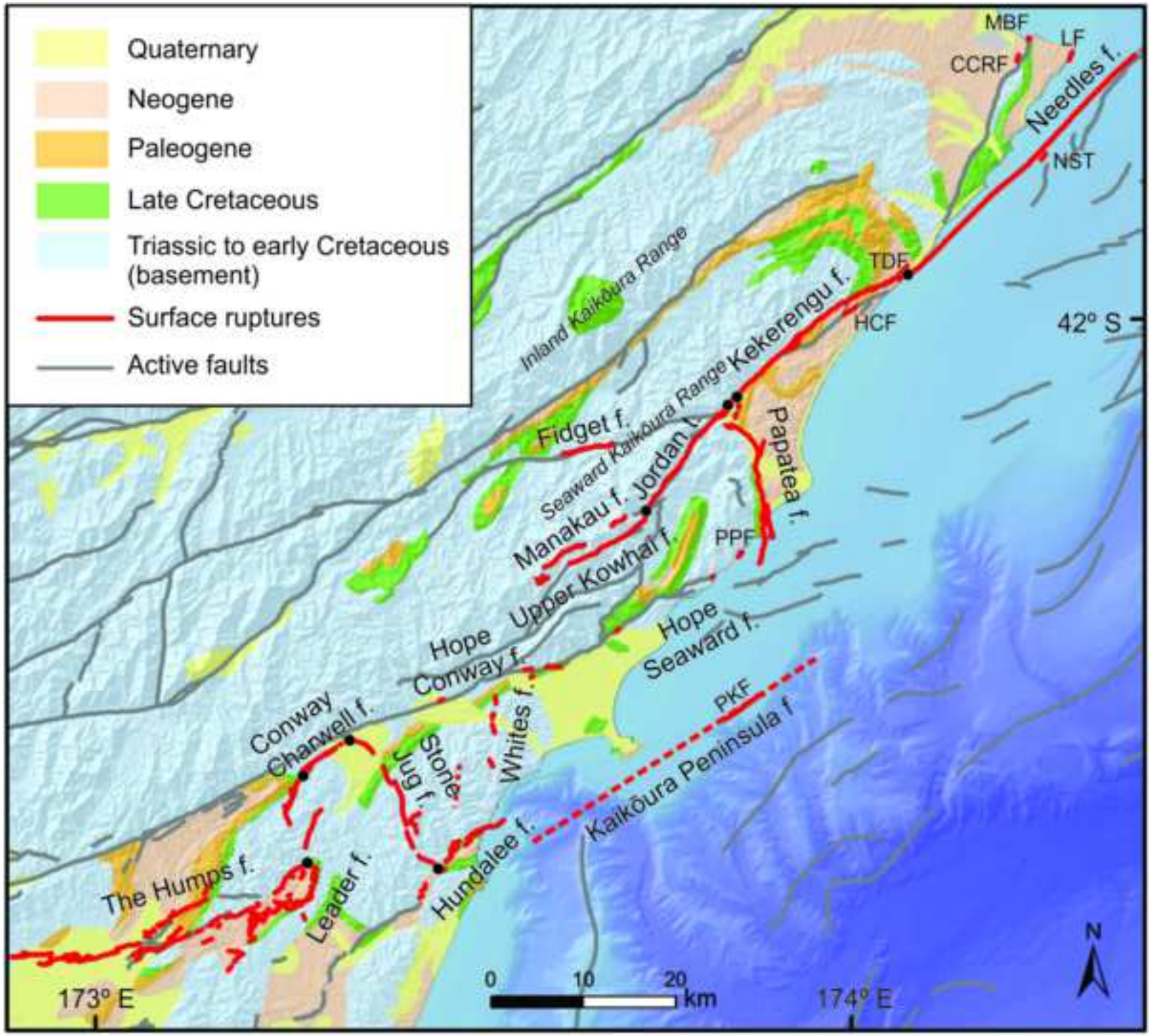

Figure 3

Click here to download Figure Fig3-Photos_Lidar.tif

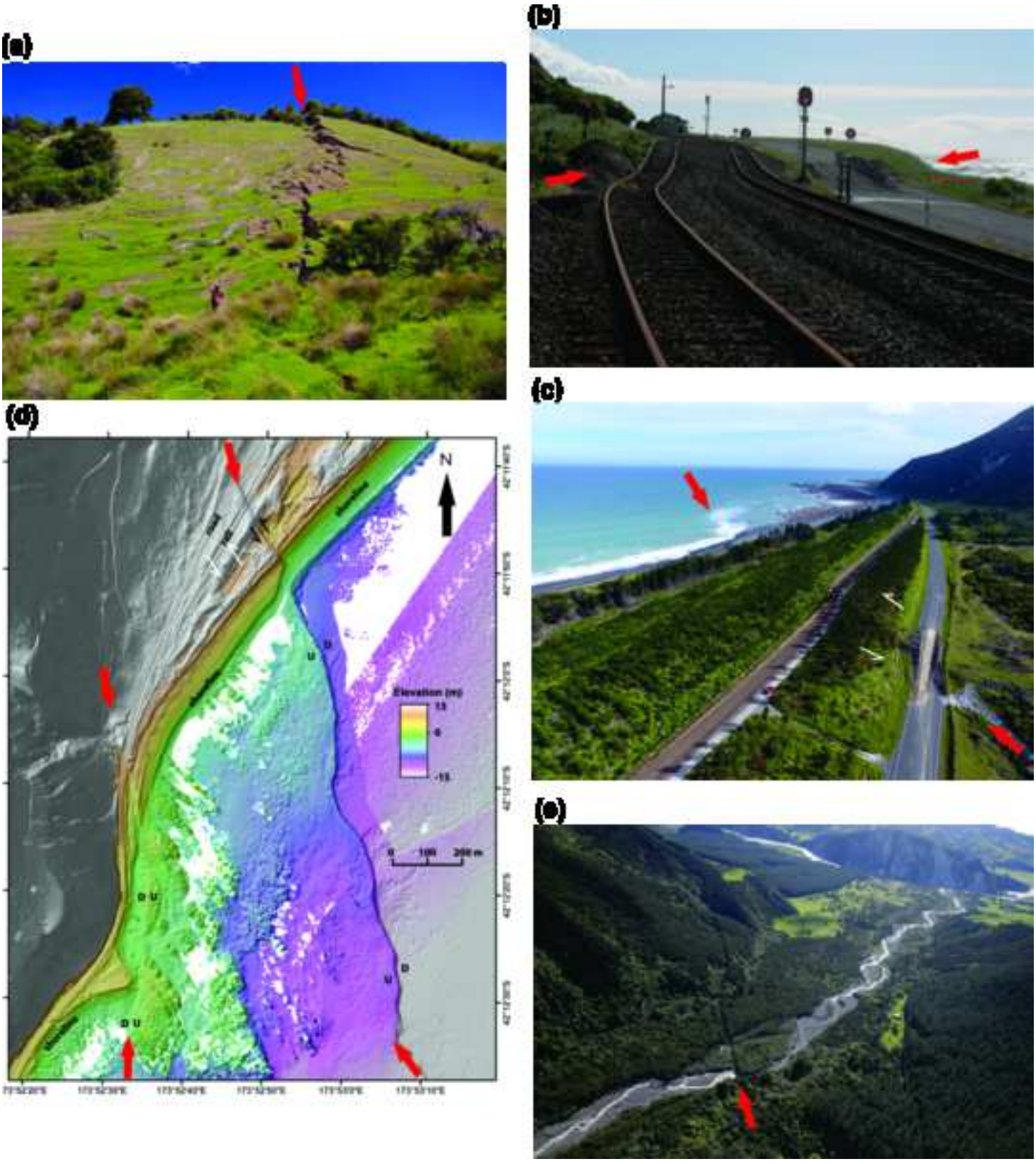

Figure 4

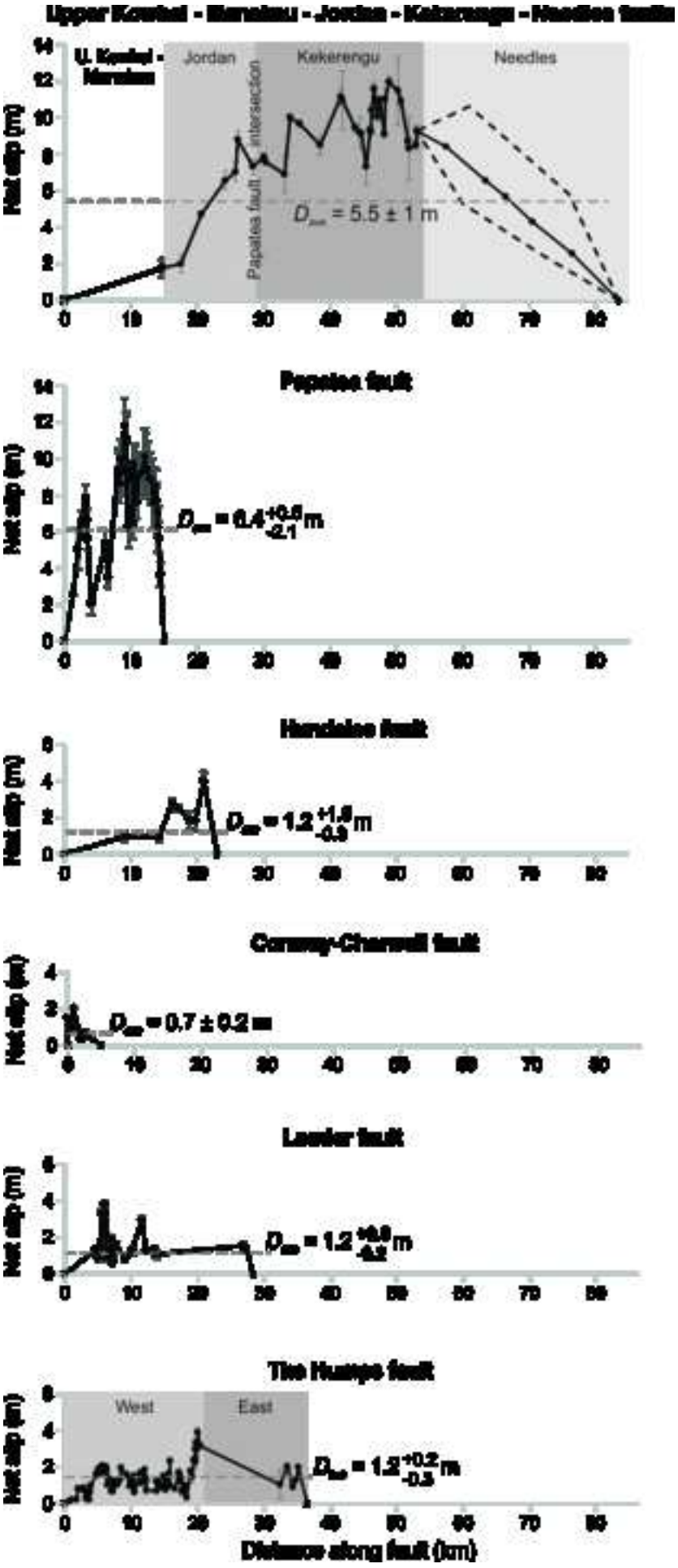

Figure 5

Click here to download Figure Fig5-3DModel.tif

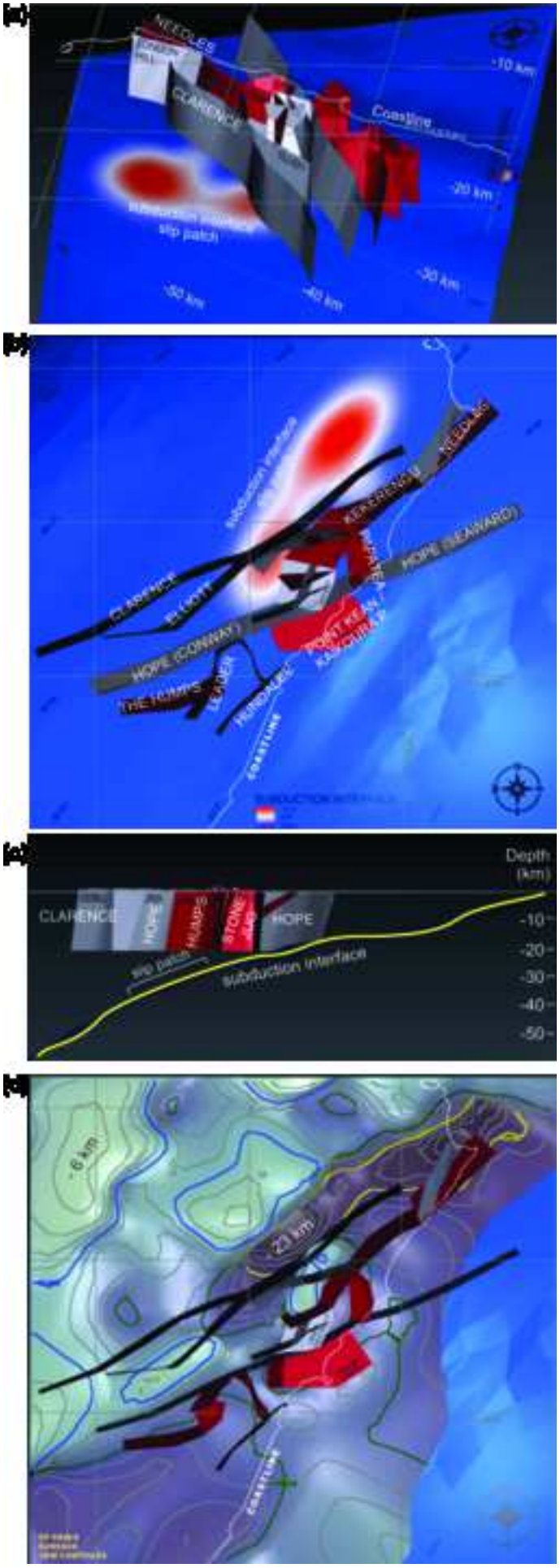

Electronic Supplement to:

Surface Rupture of Multiple Crustal Faults in the M_w 7.8 2016 Kaikōura Earthquake, New Zealand

by Nicola J. Litchfield, Pilar Villamor, Russ J. Van Dissen, Andrew Nicol, Philip M. Barnes, David J. A. Barrell, Jarg R. Pettinga, Robert M. Langridge, Timothy A. Little, Joshu J. Mountjoy, William F. Ries, Julie Rowland, Clark Fenton, Mark W. Stirling, Jesse Kearse, Kelvin R. Berryman, Ursula A. Cochran, Kate J. Clark, Mark Hemphill-Haley, Narges Khajavi, Katie E. Jones, Garth Archibald, Phaedra Upton, Cameron Asher, Adrian Benson, Simon C. Cox, Caleb Gasston, Dan Hale, Brendan Hall, Alexandra E. Hatem, David W. Heron, Jamie Howarth, Tim J. Kane, Geoffroy Lamarche, Steve Lawson, Biljana Lukovic, Samuel T. McColl, Christopher Madugo, John Manousakis, Duncan Noble, Kate Pedley, Katrina Sauer, Timothy Stahl, Delia T. Strong, Dougal B. Townsend, Virginia Toy, Jack Williams, Suzanne Woelz, Robert Zinke

The electronic supplement contains a table (Table S1) with additional data (whether the fault was previously-recognized as active, or in the National Seismic Hazard Model (Stirling et al., 2012), and the location of the maximum net surface rupture displacement) on the surface-rupturing faults. It also contains two 3D pdf figures of the 3D geological fault model (Figs. S1a and S1b). The models are identical except the second (Fig. S1b) has the addition of the *Vp* = 6 km/s isosurface (Ellis et al., 2017).

Table S1 – additional data (whether the fault was previously-recognized as active, or in the National Seismic Hazard Model (Stirling et al., 2012), and the location of the maximum net surface rupture displacement) on the surface-rupturing faults.

Figure S1a – 3D pdf of the geological fault model showing simplified major faults (this study) and the subduction interface (Williams et al., 2013).

Figure S1b – 3D pdf of the geological fault model with the addition of the *Vp* = 6 km/s isosurface (Eberhart-Phillips et al., 2017; Ellis et al., 2017).

List of Table Captions

Table S1 Additional data on the Kaikōura earthquake surface-rupturing faults, from north to south. Surface ruptures with maximum displacement >1.5 m are in bold.

List of Figure Captions

Figure S1a 3D pdf of the geological fault model showing simplified major faults (this study) and the subduction interface (Williams et al., 2013).

Figure S1b 3D pdf of the geological fault model with the addition of the *Vp* = 6 km/s isosurface (Eberhart-Phillips et al., 2017; Ellis et al., 2017).

References

Eberhart-Phillips, D., M. Reyners, S. Bannister, M.Chadwick, and S. Ellis (2010). Establishing a versatile 3-D seismic velocity model for New Zealand, *Seism. Res. Lett.* **81**, 992-1000.

Ellis, S., R. Van Dissen, D. Eberhart-Phillips, M. Reyners, J. F. Dolan, and A. Nicol (2017). Detecting hazardous New Zealand faults at depth using seismic velocity gradients, *Earth Planet. Sci. Lett.* **463**, 333-343.

Stirling, M. W., G. McVerry, M. Gerstenberger, N. Litchfield, R. Van Dissen, K. Berryman, P. Barnes, L. Wallace, B. Bradley, P. Villamor, R. Langridge, G. Lamarche, S. Nodder, M. Reyners, D. Rhoades, W. Smith, A. Nicol, J. Pettinga, K. Clark, and K. Jacobs (2012). National seismic hazard model for New Zealand: 2010 update, *Bull. Seismol. Soc. Am.* **102**, 1514-1542.

Williams, C. A., D. Eberhart-Phillips, S. Bannister, D. H. N. Barker, S. Henrys, M. Reyners, and R. Sutherland (2013). Revised interface geometry for the Hikurangi Subduction Zone, New Zealand, *Seismol. Res. Lett.* **84**, 1066-1073.

Supplemental Material (Figure S1b)

Click here to download Supplemental Material (Main Page, Tables, Figures) FigS1b.pdf

Supplemental Material (Figure S1a)

Click here to download Supplemental Material (Main Page, Tables, Figures) FigS1a.pdf